Sheaths and Double Layers with Instabilities

R. L. Stenzel[1], J. Gruenwald[2], C. Ionita[3], R. Schrittwieser[3], and J. M. Urrutia[1]

[1]Department of Physics and Astronomy, University of California Los Angeles, 475 Portola Plaza, Los Angeles, CA 90095, USA
[2]Gruenwald Laboratories GmbH, Taxberg 50, 5660 Taxenbach, Austria
[3]Institute of Ion Physics and Applied Physics, University of Innsbruck, Technikerstrasse 25/3, 6020 Innsbruck, Austria

(Received: 21. Jan. 2021, Accepted: 22. March 2021, Published online: 24. March 2021)

The properties of sheaths and associated potential structures and instabilities cover a broad field which even a review cannot cover everything. Thus, the focus will be on about a dozen examples, describe their observations and focus on the basic physical explanations for the effects, while further details are found in the references. Due to familiarity the review focuses mainly on the authors work but compared and referenced related work. The topics start with a high frequency oscillation near the electron plasma frequency. Low frequency instabilities also occur at the ion plasma frequency. The injection of ions into an electron-rich sheath widens the sheath and forms a double layer. Likewise, the injection of electrons into an ion rich sheath widens and establishes a double layer which occurs in free plasma injection into vacuum. The sheath widens and forms a double layer by ionization in an electron rich sheath. When particle fluxes in "fireballs" gets out of balance the double layer performs relaxation instabilities which has been studied extensively. Fireballs inside spherical electrodes create a new instability due to the transit time of trapped electrons. On cylindrical and spherical electrodes the electron rich sheath rotates in magnetized plasmas. Electrons rotate due to $\mathbf{E} \times \mathbf{B}_0$ which excites electron drift waves with azimuthal eigenmodes. Conversely a permanent magnetic dipole has been used as a negative electrode. The impact of energetic ions produces secondary electron emission, forming a ring of plasma around the magnetic equator. Such "magnetrons" are subject to various instabilities. Finally, the current to a positively biased electrode in a uniformly magnetized plasma is unstable to relaxation oscillations, which shows an example of global effects. The sheath at the electrode raises the potential in the flux tube of the electrode thereby creating a radial sheath which moves unmagnetized ions radially. The ion motion creates a density perturbation which affects the electrode current. If the electrode draws large currents the current disruptions create large inductive voltages on the electrode, which again produce double layers. This phenomenon has been seen in reconnection currents. Many examples of sheath properties will be explained. Although the focus is on the physics some examples of applications will be suggested such as neutral gas heating and accelerating, sputtering of plasma magnetrons and rf oscillators.

DOI: 10.31281/jtsp.v2i1.16

stenzel@physics.ucla.edu

I. Introduction

This review addresses sheaths, double layers and their instabilities. Sheaths are fundamental phenomena in plasma physics. They occur at plasma boundaries where electron and ion fluxes have to be balanced. Sheaths are also vital for understanding diagnostic probes which have been studied for nearly a century [1]. However, the instabilities associated with global effects are still a topic of research, some of which will be mentioned. As mentioned various topics will be presented in different sections, although many more effects exist. Section II describes the high frequency instability of an electron-rich sheath. Two concepts are involved, the negative rf conductance due to the electron inertia [2] and the sheath resonance due to plasma inductance and sheath capacitance [3]. The observation of the instability has been demonstrated experimentally [4]. A similar phenomenon of an ion-rich sheath near an electron emitting cathode has also been investigated [5]. Section III shows that the nonlinearity of the sheath plasma resonance can be driven unstable. A strong pump oscillation decays parametrically into half the pump frequency. Since no waves are involved the parametric instability is better described by a Mathieu equation than by three wave conservation laws [6]. Section IV describes that an ion rich sheath becomes unstable when an electron beam is injected on the electrode and emits secondary electron emission [7]. The interplay of particle currents leads to a negative differential current-voltage characteristics. When

the current closes through a resonant circuit it starts to oscillate with large amplitudes. It is an example of the importance between an unstable sheath and the global circuit to excite an instability. Section V demonstrates that injecting an ion beam into an electron-rich sheath widens the sheath and can create a double layer [8, 9]. Vice versa, in Section VI, a plasma expansion into vacuum forms a propagating ion-rich sheath. When two populations of electrons exist the slow electrons reflect which modifies the sheath form a stationary current-free collisionless double layer [10, 11].

Further sections show additional sheath properties with instabilities. For example, in the presence of neutrals ionization can arise in electron rich sheaths [12]. The ion creation results in broadening the potential profile until forming a double layer at the boundary as a visible "fireball" or "anode glow" [13, 14, 15, 16]. Various instabilities arise, such as fireball relaxation instabilities and electron transit time instabilities [17, 18]. In magnetized plasmas electron rich sheaths can rotate due to $\mathbf{E} \times \mathbf{B}_0$ drifts which forms electron drift wave eigenmodes [19]. Inverted fireballs can be formed with positively biased spherical electrodes consisting of a highly transparent grid so that electrons are focused into a sphere [20, 21]. The grid potential drop forms a double layer whose potential can be much higher than the ionization potential. The grid can also be reversed so as to inject energetic ions into the sphere. The impact on the grid ejects secondary electrons which become confined inside the sphere. Ionization in an electron-rich sheath can produce sheath modifications which affect many other instabilities [22]. Negatively biased permanent magnets also form sheaths, secondary electrons and plasmas, known as magnetrons and used for sputtering [23, 24].

Some instabilities arise only in the sheath, others depend on global effects, i.e., depend on the surrounding plasma or current closure path. For example, a positively biased probe in a magnetizes plasma produces an ion relaxation instability [25]. The electrode raises the potential in the flux tube relative to the ambient plasma which forms a radial "sheath". When the flux tube is positive the weakly magnetized ions are expelled, the current collapses, the radial electric field reverses and the ions return. This process repeats as a relaxation oscillation which is driven by local and global sheath effects free of ionization effects. The current disruptions also arise in magnetic reconnection experiments. Due to ion expulsion the anode current collapses, produces a large inductive voltage which forms a double layer [26]. The role of secondary electron emissions plays an important role in the sheath physics. For example, the spherical grid electrode has been biased strongly negative to repel external electrons. However, ions are accelerated into the sphere and creates secondary emission by ion impact at the grid. Thus, the cold electrode is a cathode, emitting electrons and collecting ions injecting from the ambient plasma. A plasma with negative potential can be formed without ionization inside this sphere. The focus at the center creates a dense hot plasma which led to the concept of "fusor" devices [27]. On solid electrodes with strong negative bias the secondary electron emission can develop into sputtering effects. Small surface spots melt and ionize the solid metal which provides a cathode supplying large currents and dense plasmas. Sputtering plasmas are difficult to diagnose since they occur randomly in space and time with variable properties and too small for diagnostic probes. Sputtering is used for coating applications [28, 29].

II. Transit time instability of the sheath-plasma resonance

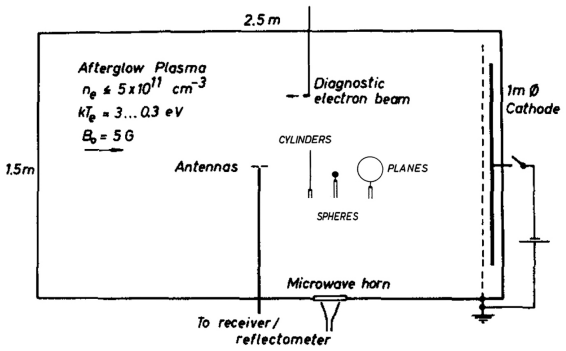

Figure 1: Schematic diagram of the experiment on sheath-plasma instabilities. Electrodes of different geometries produce instabilities at the sheath-plasma resonance near the plasma frequency and the ion-plasma frequency. A diagnostic electron beam is used to measure the electron plasma frequency accurately. Figure reprinted from reference [4].

A positively biased electrode has been observed to excite high frequency oscillations near the electron plasma frequency [4]. This instabilities are observed in a large quiescent afterglow plasma shown schematically in Fig. 1. The high frequency instability occurs below but close to the electron plasma frequency. It occurs on electrodes of different geometries, although with slightly different frequencies. The sheath-plasma resonance arises from the capacitive sheath and the inductive

plasma response. The instability arises from the inertia of electrons passing through the sheath which can also be explained by the negative differential resistance of the L-R-C sheath circuit. The instability is not an "orbitron" oscillation [30] which describes electron rotations around a cylindrical electrode without relation to the sheath-plasma resonance. The latter arises on plane and spherical electrodes.

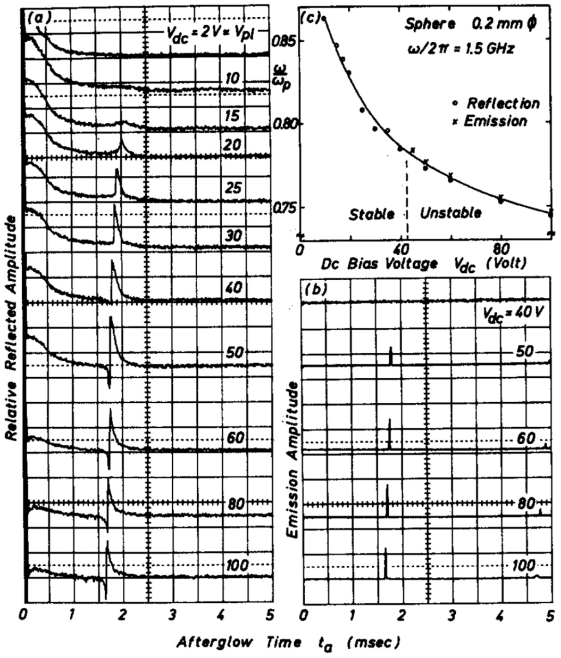

Figure 2: (a) Sheath-plasma resonance obtained from a reflection measurement of a test wave. The density is varied in the afterglow while the frequency is constant. The resonance is pronounced for electron rich sheaths. (b) Under identical conditions the sheath excites an instability at the same frequency as the reflection line. (c) Frequency of the measured reflection and emission lines for different dc bias, except not below the instability threshold. Figure reprinted from reference [4].

Fig. 2 shows the properties of the sheath-plasma instability. The sheath-plasma resonance is visible from the peak of the reflected signal of a test to the coax-fed electrode [Fig. 2 (a)]. The frequency is fixed ($\omega/2\pi = 1.5$ GHz) while the plasma frequency (ω/π) decreases in time which tunes through the resonance line. Increasing the electrode bias increases amplitude and decreases the normalized frequency (ω/ω_{pe}) due to widening the sheath. Fig. 2 (b) shows the emission from the electrode whose emission line coincides with the sheath-plasma resonance. Fig. 2 (c) summarizes the signal dependence on dc voltage which confirms an instability threshold ($V_{dc} \simeq$45 V). At large electrode voltages the instability exhibits harmonics, which can arise from electron bunching. While the fundamental is confined to the sheath the harmonics with $\omega > \omega_p$ can propagate and are observed external to the plasma.

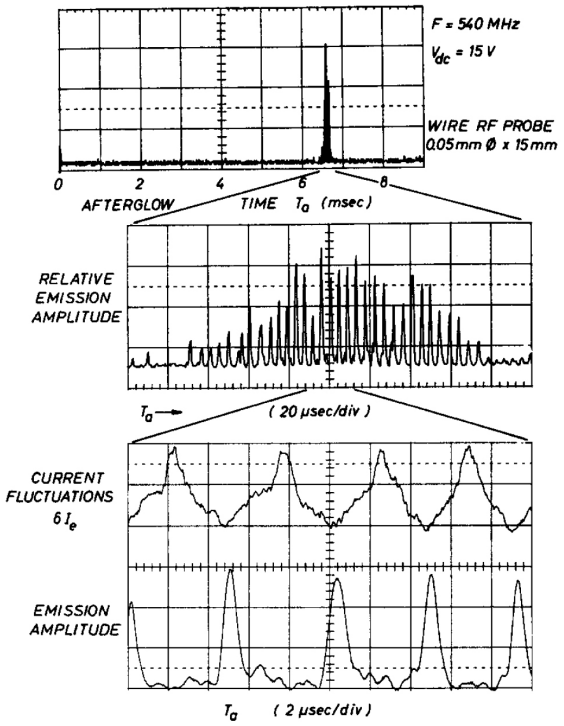

Figure 3: Time resolved high frequency sheath-plasma instability. Line broadening is visible on the large time scale ($\propto \omega/\omega_{p,t}$) which appears as many sidebands on an expanded scale. Further expansion to the microsecond time scale shows that the rf instability occurs in bursts with $\simeq 5\mu$s repetition time, the travel time of ions through part of the sheath. The current to the electrode exhibits the same fluctuations which could arise from a sheath width modification due to injected and reflected ions . Figure reprinted from reference [4].

Close inspection shows that the high frequency signal is modulated by a low frequency signal as shown in Fig. 3. Expanding the frequency scale gives the impression of many sidebands but further time resolution shows that the rf amplitude oscillates in time. Both the electrode current and rf amplitude repeats at a frequency close to the ion plasma frequency. Similar repetitive electrode currents have been observed earlier [31] and will be shown further below.

III. Parametric instability of the sheath plasma resonance

In an unmagnetized discharge plasma the sheath-plasma resonance has been studied differently. In-

stead of creating the instability an external rf signal is applied to study the nonlinearity of the sheath resonance [6]. The setup is shown in Fig. 4 (a), where the short, coax-fed wire tip forms the electrode. It is oscillated by a high frequency "pump" signal, coupled via a capacitor to the floating rf electrode. Incident and reflected signals are obtained from directional couplers. The applied rf pump is pulsed with slow rise time in order to observe the onset of instabilities.

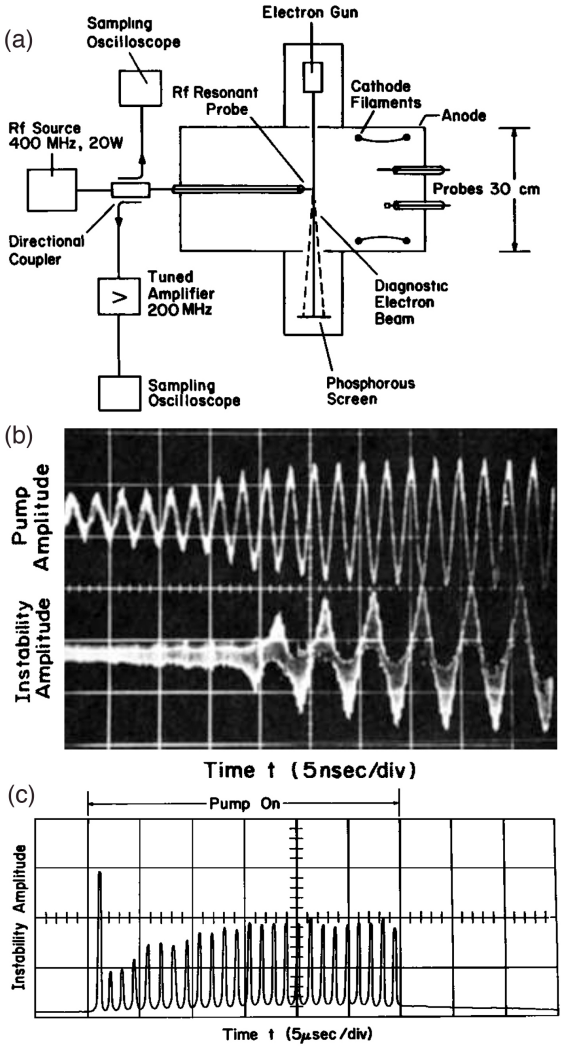

Figure 4: (a) Schematic diagram of the experimental setup. Typical plasma parameters are density $n_e < 10^{10}$ cm^{-3}, electron temperature $kT_e \simeq 2$ eV, Argon pressure $p = 4 \times 10^{-2}$ Pa, device diameter 30 cm and length 40 cm. (b) Simultaneous traces of the pump waveform (top) and the decay waveform (bottom) at half the pump frequency. (Rf amplitude at threshold V_{rf}=10 V, pump frequency $\omega/2\pi = 420$ MHz). (c) Envelope of the rf instability ($|V_{rf}|$) on a slow time scale showing that the sheath also oscillates near the ion plasma frequency. Figure reprinted from reference [6].

Figure 4 (b) shows the rising oscillation of the 400 MHz pump . At a certain threshold (10 V at the probe) the reflected signal at half the pump frequency is excited. It is phase locked. The sheath nonlinearity produces a parametric instability. The latter is commonly understood by three-wave interaction, satisfying energy ($\omega_{pump} = \omega_1 + \omega_2$) and momentum ($\mathbf{k}_{pump} = \mathbf{k}_1 + \mathbf{k}_2$). Neither pump nor decay waves can propagate, thus the instability is not convective. Since the oscillation is confined to the sheath it is an absolute instability. An earlier explanation is that the large rf electric field oscillates the sheath thickness s, given by $\omega_r = \omega_p[s/(R+s)]^{1/2}$, where R is the radius of the spherical electrode [3]. The oscillation amplitude y(t) can be described by a Mathieu equation

$$d^2y/dt^2 + \omega_{r0}^2(1 + \epsilon \sin\omega_0 t)y = 0 \qquad (1)$$

where ϵ is proportional to the pump amplitude and $\omega_{r,0} = \omega_r$ for $\epsilon = 0$. The instability with lowest threshold arises when the decay mode has half the pump frequency, $\omega_0 = 2\omega_{r,0}$, as is shown in Fig. 4 (b). The nonlinearity of the sheath-plasma resonance produces both a sub harmonic and higher harmonics [4].

IV. Secondary electron emission instabilities

A gridded electrode is immersed into a dc discharge plasma without magnetic field. An electron beam impacts the grid which releases secondary electrons [Fig. 5 (a)] [7]. The emission current depends on the grid voltage. For a large negative grid voltages with amplitudes $V_{grid} > V_{beam}$ all ions are collected and all electrons are reflected. For $V_{grid} < V_{beam}$ the incident electrons are collected which reverses the sign of the current at the first floating potential, $V_{f,1}$. Ion collection and secondary electron emission have the same sign causing another current reversal or floating potential $V_{f,2}$. Approaching the plasma potential the collection of abundant low energy electrons are collected which leads to a third current reversal or floating point $V_{f,3}$ [Fig. 5 (b)].

When dI/dV is negative the current becomes unstable. The potential of a floating grid becomes stable at the first and third current zero crossings, but is unstable at the second zero current. In order to force stability the external circuit resistance must be smaller than the resistance of the sheath. If the load is reactive an $L - C$ circuit will oscillate as shown in Fig. 5 (c). The grid voltage is slowly raised from V_{beam} to V_{plasma} while the grid is oscillating between the two outer stable current

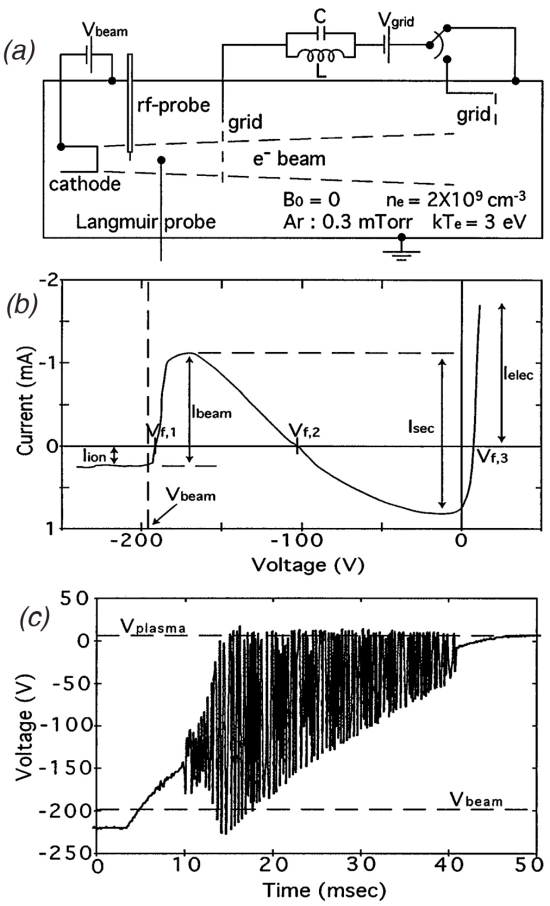

Figure 5: (a) Schematic diagram of the experiment and basic plasma parameters. (b) Current-voltage characteristics of the gridded electrode which emits secondary electrons. The negative differential resistance results in oscillations when a resonant circuit closes the current circuit. (c) The grid voltage is slowly raised which leads to grid oscillations between the two outer floating potentials. Frequency and amplitude depend on the global circuit. Figure reprinted from reference [7].

null points. The frequency is determined by a series resonance frequency. The oscillation can be tuned externally. Its amplitude is much larger than that of the sheath oscillations. Although the sheath is the source of the instability the global circuit is vital for the instability properties.

V. Ion injection into electron rich sheath producing sheath expansion and double layer

The following experiment deals with the injection of ions into an electron-rich sheath which leads to sheath expansion and double layer formation [8, 9]. Figure 6 (a) shows an ion beam which is injected into an electron-rich sheath of a positively biased electrode. Different positive ions have been used, but no negative ions. When the beam voltage is smaller than the positive voltage of the disk electrode, ions penetrate, slow down, stagnate and reflect. Flux conservation implies that the ion density peaks at the stagnation point inside the sheath. A large ion density gives rise to an ion-rich sheath next to the electron rich sheath, resulting in a double layer. The double layer can be easily seen in Fig. 6 (b) by the dense spacing of the equipotential lines on the ion beam side. On the opposite side of the magnet the potential drops closely to the electrode surface in a thin electron-rich sheath. The potential drop at the double layer and the neutral pressure is too low to produce ionization. Likewise no fireball is formed at the left side of the magnet. By increasing the ion beam density or velocity the double layer shifts toward the magnet and forms a V-shape similar to auroral double layers. On axis of the magnet the electrons are collected along $\mathbf{B}_0$, off axis the electrons perform $\mathbf{E} \times \mathbf{B}_0$ drifts and gain no energy.

The double layer potential scales proportional to the ion beam energy, implying that the DL is due to ion beam stagnation. This is fundamentally different from a sheath expansion due to ionization of neutrals, called a fireball [18]. The potential drop of fireball double layers is close to the ionization energy level necessary to balance the particle inflow and outflow. The ionization is accompanied by excitation which causes the light emission. However, the collisionless DL due to ion beam injection produces no visible light.

Figure 7 (a) shows potential profiles with and without double layer. The double layer potential scales proportional to the ion beam energy, implying that the DL is due to ion beam stagnation. Ion beam generated double layers can be produced below the ionization potential hence cannot produce ionization. For large double layer potentials no visible light is seen as in collisional fireballs. Figure 7 (b) shows evidence for potential fluctuations which are only observed in the double layer but not in the surrounding plasma with constant potential. The fluctuations have a broad spectrum below the ion plasma frequency. However, they do not excite ion acoustic waves, hence are fluctuations in the double layer due to unstable density and double layer position. Since the ions are totally reflected the double layer resembles a "virtual anode" for ions which is unstable at the ion transit time. Fluctuations at the grid of double plasma devices have been observed similar effects [31] .

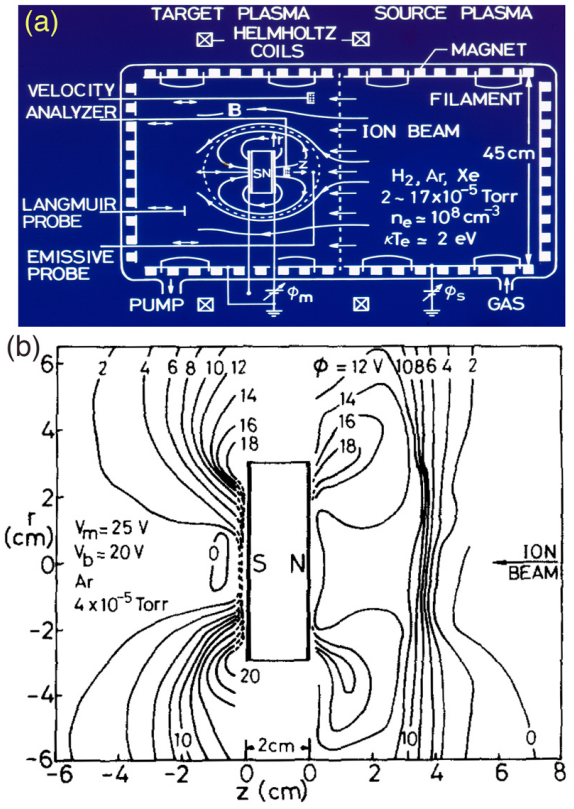

Figure 6: (a) Schematic diagram of the experiment setup and basic plasma parameters. The double-plasma device generates in the right half chamber an ion beam. In the left half chamber a positively biased permanent magnet produces an electron rich sheath. The ions reflect from the sheath potential and forms a fireball without ionization. (b) Equipotential lines show the double layer on the right side, a thin sheath on the left side without beam ions. Figure reprinted from reference [8, 9].

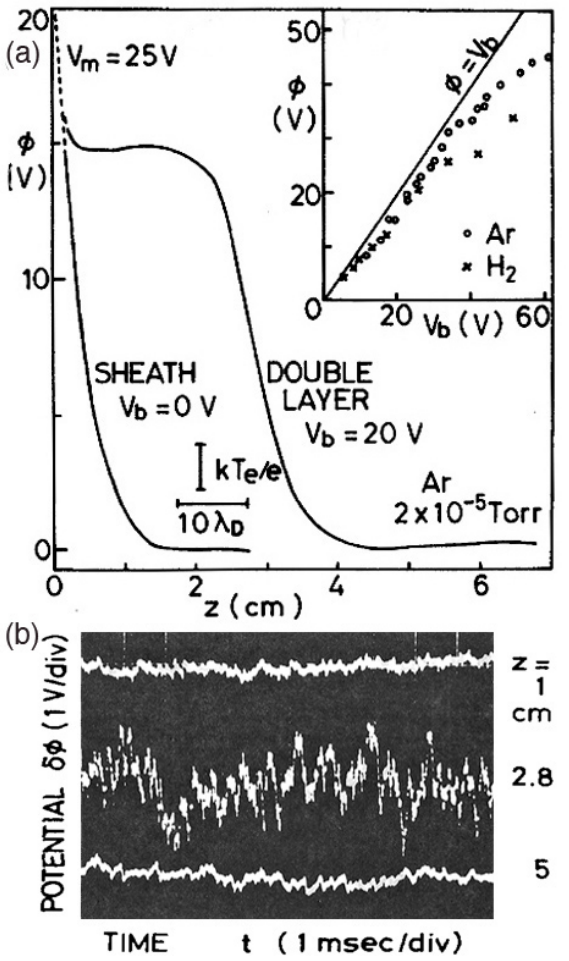

Figure 7: (a) Plasma potential with and without injected beam ions. With increasing beam penetration the sheath widens and forms a double layer. The insert shows that the double layer potential scales with beam energy. No fireball is formed since ionization cannot arise for low gas pressure and for potential drops smaller than the ionization energy, hence no light is seen for this "fireball". (b) Inside the double layer fluctuations in the sound wave regime are observed, but no ion waves are outside the double layer. The double layer may be unstable in position and/or amplitude. Figure reprinted from reference [9].

VI. Free plasma expansion into vacuum with a moving sheath and a stationary double layer

The free expansion of plasma into vacuum exhibits a moving sheath and and a stationary double layer [10, 11]. Figure 8 (a) describes the experimental setup and Fig. 8 (b) shows the evolution of the potential profile at turn-on of the expansion process. The sheath develops to slow down the fast electrons while accelerating the ions, thereby establishing no currents and nearly charge neutrality. The sheath is varying in space and time when the plasma starts to expand. A double layer arises in the dc discharge where two species of electrons exist, a low density population of energetic primary electrons and a dense but low energy secondary electrons produced by ionization. The early potential drop between the source and the expansion front is determined by the energetic electrons. The decreasing potential is a moving ion-rich sheath. The low energy electrons cannot reach the front since the potential drop of the fast electrons is too large. As the secondary electrons slow down, stagnate and reflect a double layer is formed. It has a potential drop of a few times the secondary electron energy. It can be interpreted as an injection of electrons into an ion rich sheath resulting in flattening the potential profile and the formation of a double layer. Except for the sign of the charge the physics is the same as the injection

of ions into an electron-rich sheath [8]. However, the present case differs from weak double layers observed in helicon plasmas expanding along a diverging magnetic field [32].

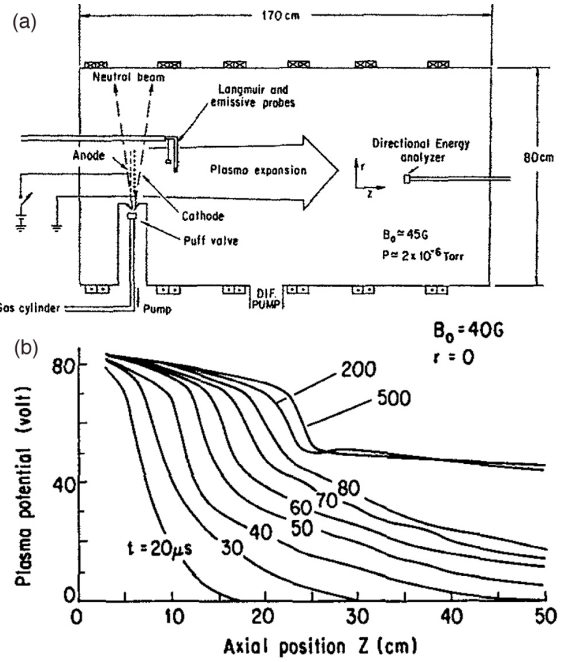

Figure 8: (a) Experimental setup for studying the free plasma expansion into vacuum. A neutral beam is pulsed radially through the dc discharge while the plasma expands axially along a uniform dc magnetic field into vacuum. (b) Plasma potential vs axial position and time, showing an expanding negative potential (ion rich sheath) due to the energetic primary electrons. In time the low energy secondary electrons reflect which forms a stationary double layer. The negative potential is an ion-rich sheath into which the low electrons stagnate and form a double layer, similar to the injection and reflection of ions into an electron-rich sheath which forms a double layer at the stagnation point. However, the expansion into vacuum is current free since ions and electrons expand together which produces very fast ions at the front. The double layer potential drop differs from fireballs since ionization plays no role in vacuum. Figure reprinted from reference [10].

Compared to anode fireballs the double layer in an expanding plasma is current free since there is no "electrode" to close the current. It is the sheath which establishes equal flow of electrons and ions. In the direction of expansion the ions are accelerated which implies a density decrease due to flux conservation. If the source plasma is constant the double layer is also stationary, whereas the expansion continues to stretch the potential profile.

Instabilities can also arise in expanding plasmas. Low frequency broadband fluctuations are observed downstream of the double layer [Figs. 9 (a,b)]. Cross-correlations show propagation speed and direction which indicates convection of the fluctuations [Figs. 9 (c,d)]. The fluctuations may arise in the double layer where the secondary electrons totally reflect at a virtual cathode ("vircator" [33]) which produces oscillations due to electron inertia. Upstream of the double layer the counter propagating electrons may cause beam instabilities. Furthermore the plasma source is a dc discharge which is not current free and may produce current-driven ion sound instabilities. The ion outflow may convect instabilities downstream.

Another case of double layer formation arises in an inverse fireball which will be explained further below.

VII. Rotating electron-rich sheath with electron drift wave instability

In a uniform magnetic field $\mathbf{B}_0$ the electron-rich sheath differs from the direction of $\mathbf{E}$ and $\mathbf{B}_0$ [19]. For a spherical electrode with positive bias the radial electric field is perpendicular to the magnetic field in the equatorial plane as seen in Fig. 10 (a). The electrons perform an $\mathbf{E} \times \mathbf{B}_0$ drift around the equator while at the poles they encounter $\mathbf{E} \parallel \mathbf{B}_0$ where the electrons are collected as for $\mathbf{B}_0 = 0$. The electron density at the equator exceeds that at the poles which produces the visible glow. No fireballs are observed at the poles. The drifting electrons support perturbations which reinforce when the drift waves have integer wavelengths around the sphere ($n\lambda = 2\pi R$). These eigenmodes dominate the fluctuation spectrum. With a tuned amplifier the waveform of the probe oscillations are shown vs time and equatorial position [Fig. 10 (b)]. The waves travel in the drift direction and have two periods per circumference, hence is identified as an m=2 eigenmode. Figure 10 (c) shows the eigenmode spectrum for large dc bias (180 V). It exhibits a large number of eigenmodes, although the amplitudes are shown on a logarithmic scale. The waveform of the raw probe signal, shown in the insert, depicts a non-sinusoidal waveform. The waveform may arise from electron bunching and variations in drift speed since the electric field depends on radius and polar angle.

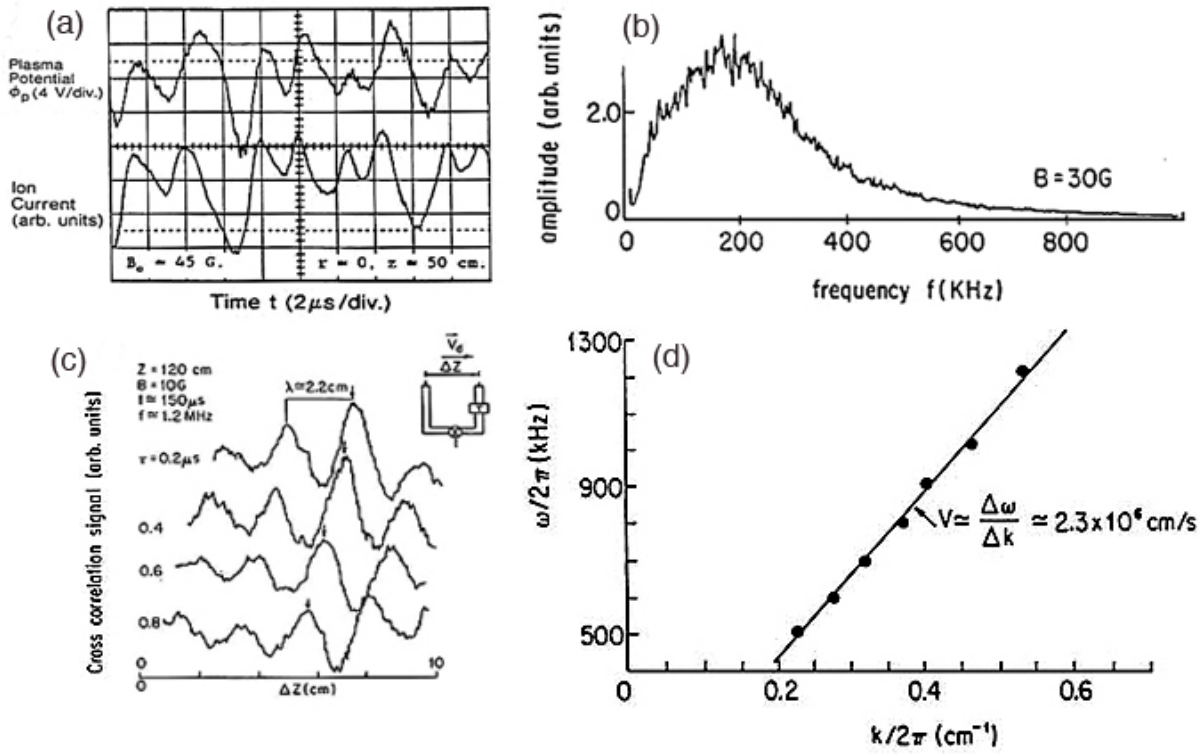

Figure 9: Instabilities during plasma expansion into vacuum. (a) Fluctuations in time of correlated potential and density fluctuations characteristic of sound waves. (b) Frequency spectrum indicates broadband fluctuations in the ion sound regime. (c) Spatial dependence of fluctuations measured by narrowband cross correlations. The waves propagate in the direction and speed of the plasma expansion. (d) Dispersion relation of the turbulence indicates a sound wave riding on an expanding plasma flow. Figure reprinted from reference [11].

VIII. Relaxation instabilities of positive electrodes in magnetized plasmas

The following experiment shows that a classical electron sheath cannot explain the observed instability in a weakly magnetized plasma [25, 34]. Figure 11 (a) shows the current waveform which exhibits first a large current pulse (80 A) followed by repeated current pulses. The slow pulse repetition (5...10 μs) is of order of the ion transit time through the flux tube of the disc electrode (2 cm diam.). Figure 11 (b) shows the density profile vs time at 1 cm in front of the electrode. The ions are radially accelerated at the sound speed by an electric field across $\mathbf{B}_0$. After the first density depression the current creates a minimum. When the current collapses the plasma pressure partly refills the density depression and a new current spike develops. The plasma dynamics creates a relaxation instability which depends not only on the sheath but on the global electric fields and current propagation.

A classical sheath in an unmagnetized plasma is located parallel to a plane disk electrode. However, observations show that the disk potential does not vanish beyond a few Debye length. The potential extends along $\mathbf{B}_0$ and creates a radial electric field well outside the sheath. The magnetized electrons perform an $\mathbf{E} \times \mathbf{B}_0$ drift, while the unmagnetized ions respond to the electric field. The ion dynamics across the flux tube of the electrode controls the collected current. Another unexpected feature is the first large current pulse. The insert in Fig. 11 (a) shows that the current scales almost linearly with applied voltage to the probe. The peak value exceeds the classical electron saturation current by at least an order of magnitude, implying that a different physics matters, which is a wave phenomenon. By measuring the perturbed magnetic field in three dimensions one obtains the current density in space and time. Figure 11 (c) shows that the current flows in a gradually expanding spiral along $\mathbf{B}_0$ similar to a magnetic flux tube. The current front is carried by a low frequency whistler mode packet. Before the current reaches the chamber wall the current has a coaxial return current to the back wall. The current is a wave current, dominated by Hall physics, rather than the classical model of a thermal electron flux into the electrode sheath. The current is driven by inductive electric fields and space charge fields. The former

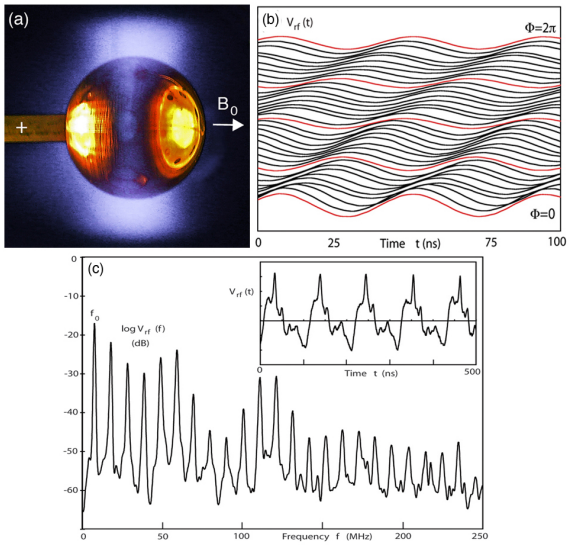

Figure 10: Instability of a rotating electron-rich sheath which produces electron drift waves. (a) Picture of a positively biased spherical electrode which exhibits sheath electrons in the equatorial plane. The radial sheath electric field and the axial magnetic field causes an $\mathbf{E} \times \mathbf{B}_0$ drift. Unstable drift waves form azimuthal eigenmodes. (b) Wave potential vs time at different azimuthal positions show direction of propagation and two wavelengths around the sphere, i.e. an m=2 mode. (c) A wide spectrum of eigenmodes are observed for a large dc bias which creates electron bunching (see insert). Figure reprinted from reference [19].

arise from time-varying magnetic fields, the latter are caused by space charge imbalances between mobile electrons and slow ions. The pulsed electrode acts like an antenna and the current collected is a wave current [34, 35, 36].

When the large current peak collapses the ions respond to electric fields but not magnetic fields in Hall physics. Figure 11 (d) shows that the rise and decay of a large current pulse creates strong inductive voltages on the electrode. The inductance arises from the transmission line between the power supply (V_0) and the electrode (V_{el}). When the current collapses the electrode voltage rises above the constant supply voltage. The voltage increase enhances the density depletion leading to a faster current collapse. After the loss of the current the pressure gradient partially reverses the ion depletion. The current recovers and the process repeats at a rate given by the ion transit time in and out of the current channel. Thus, the relaxation oscillation instability involves the electron sheath dynamics, Hall electric fields and ion flows, none of which can explain the instability alone. When the rise time of the electrode voltage is slowed down the initial current pulse decreases and vanishes, but all other relaxation peaks remain the same. Thus, the instability is not a ringing response to the first pulse but a genuine instability. On the other hand a rapid sweep of a Langmuir probe exhibits a current spike at the plasma potential. This overshoot effect can lead to erroneous interpretations. For small probe voltages and small probe areas the overshoot effect vanishes. The experiments were performed at a low neutral pressure (5×10^{-2} Pa) where ionization did not occur. However when the pressure is increased by an order of magnitude the light from fireballs is observed. The current rise time is slow and exhibits no relaxation instabilities.

Another example for current disruptions has been observed in magnetic reconnection experiments [26]. Fig. 12 (a) shows that a current sheet has been established by applying an inductive electric field along a magnetic guide field in a large dense plasma column. The current (400 A) flows between a coated cathode and a grounded anode end plate. In order to increase the current density a smaller end plate has been biased positively. Fig. 12 (b) shows the waveforms of current and voltage for the inner small anode. Without bias the current waveform is a half cycle of 1 ms duration. When biased to +10 V the current disrupts spontaneously several times. Note that the fast drop of a large current produces an inductive voltage several times larger than the applied dc voltage. A fraction of the large anode voltage drops off in the anode sheath, the rest forms a double layer well away from the end anode [Fig. 12 (c)]. The double layer does not qualify as a "fireball" since the potential drop exceeds the ionization potential and there is no light emission or ionization. Further observations show that the disruption of the small anode current is compensated by an increase of the large anode. Thus the total current is not disrupted. Neither the single anode nor the large anode nor both connected together show no disruptions. Thus the disruption is local near the small anode. The neutral sheet is modified between an X-type (current disruption) and O-type (max current) null points. The current disruption appears to be a result of magnetic fields rather the cause. The physics is similar to that of the relaxation instability where the positive disk expels plasma and disrupts the current [26]. Both the sheath and the global current system are coupled which needs to be further investigated since reconnection models rarely consider boundary effects.

IX. Sheath instabilities with ionization

When an electron rich sheath has a potential exceeding the ionization potential and the neutral density is increased both ionization and excitation

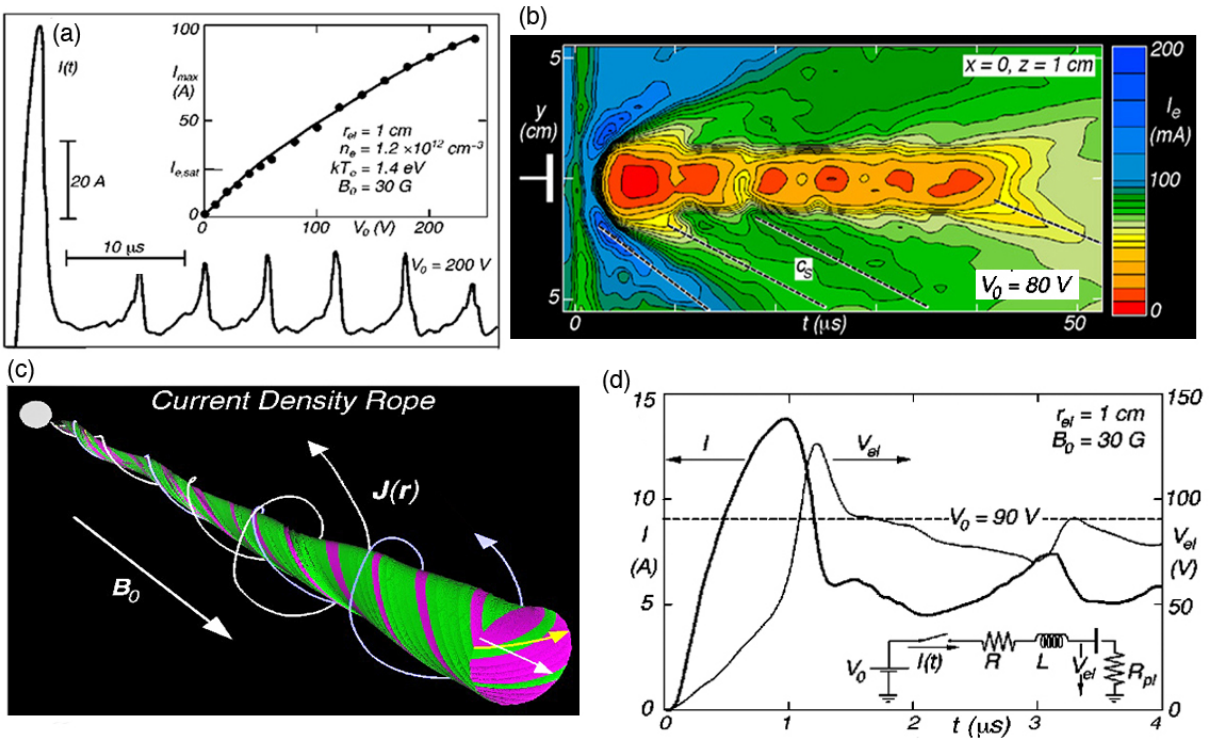

Figure 11: Relaxation instabilities arise when an electrode collects electrons in a weakly magnetized plasma. (a) Current waveform showing first a large overshoot followed by smaller peaks. (b) Density contours vs radius and time just before the electrode. The first overshoot depletes the density near the probe, followed by smaller density modulations. The ion expulsion occurs at the sound speed. (c) The measured current density forms a spiraling rope along $\mathbf{B}_0$. (d) The waveforms of the first electrode current and voltage indicating strong inductive effects. The current circuit has inductive and resistive components which affect the instability. Figure reprinted from reference [25, 34].

occur inside the sheath. At threshold conditions the ionization events are sporadic. The ionized particles are accelerated in different directions and with different speeds. Electrons rapidly move toward the electrode, ions move much slower away from the anode into the ambient plasma. The slow ions form a excess positive space charge which broadens the sheath potential [12]. Without ionization the sheath excites the high frequency sheath-plasma instability. When the sheath widens due to ionization the high frequency instability is affected, frequently quenched as shown in Fig. 13 (a,b). Ionization increases the electron current which indicates density changes. After each ionization event the density and the high frequency decay. Figure 13 (c) shows a sheath which is expanded due to ionization. It is an intermediate case between an invisible collisionless sheath and a bright large fireball. Note that the sheath ionization leads to a chain of instabilities such as modulation of the high frequency sheath instability (Fig. 13a), formation of fireballs (Fig. 14a) which exhibit low frequency relaxation oscillations (Fig. 15a).

X. Electron-rich sheaths developing into fireballs

When the electrode potential is raised above the ionization potential the energetic electrons in the sheath ionize which creates secondary electrons and ions as in dc discharges [Figs. 14 (a,b)]. Ions from the ambient plasma cannot enter the fireball. Ions produced inside the fireball are expelled at the potential drop. They are also lost at the electrode which requires an ion rich sheath to balance ion and electron losses. The size, location and stability of the double layer depends on the balance between production and losses. For plane electrodes the shape of the fireball is usually spherical [16, 18]. In a uniform magnetic field the fireball turns into a cylindrical "firerod" [13]. Many other shapes arise in mirror or cusp magnetic fields [16]. In Fig. 14 (c) the electrode is a cylindrical grid and the fireball is formed on the inside due to geometrical focusing. This suggests that the fireball can be confined inside a spherical electrode. Figure 14 (d) shows that a highly transparent spherical grid can trap a fireball on the inside [21, 22]. This "inverted" fireball has interesting and new properties. First, the

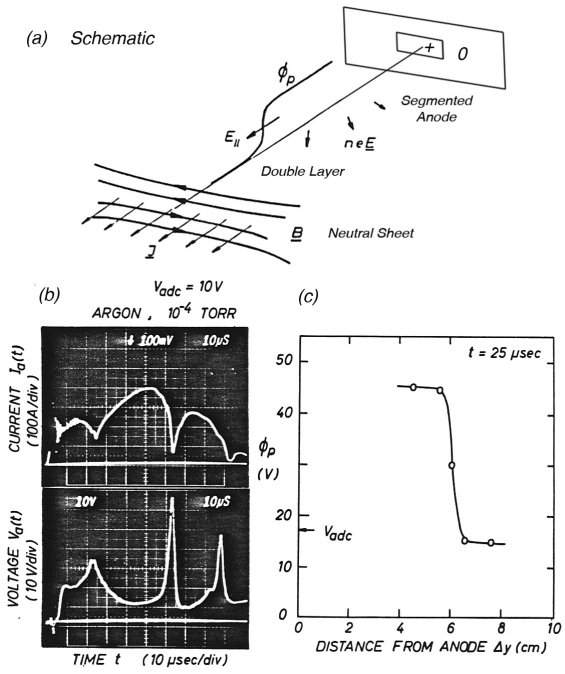

Figure 12: Current disruptions and double layer formation in magnetic reconnection. (a) Schematic setup. (b) Waveforms of current and voltage of the small electrode biased 10 V positive with respect to the grounded outer anode. Spontaneous current disruptions create large induced voltages spikes. (c) Plasma potential shows the formation of a double layer axially away from the small anode. At the double layer the particles are accelerated on expense of the magnetic energy stored by the current. Figure reprinted from reference [26].

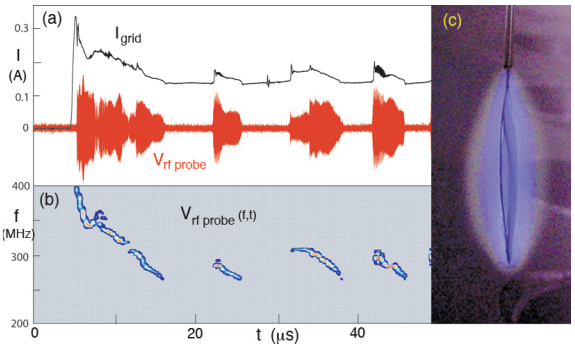

Figure 13: (a) Waveforms of two different instabilities of an electron-rich sheath prior to the fireball formation ($V_{grid\ dc}$ =45 V, 5×10^{-2} Pa, Ar). The low frequency spikes in the grid current are caused by ionization in the sheath. The high frequency bursts are due to the sheath-plasma resonance instability. (b) Spectrum of the high frequency oscillation showing the decrease in frequency as the grid current or density decays. (c) Picture of a widened sheath with erratic ionization events, not time-resolved by a picture. The light is due to electron-neutral excitation. The color change indicates the electron energy. Figure reprinted from reference [12].

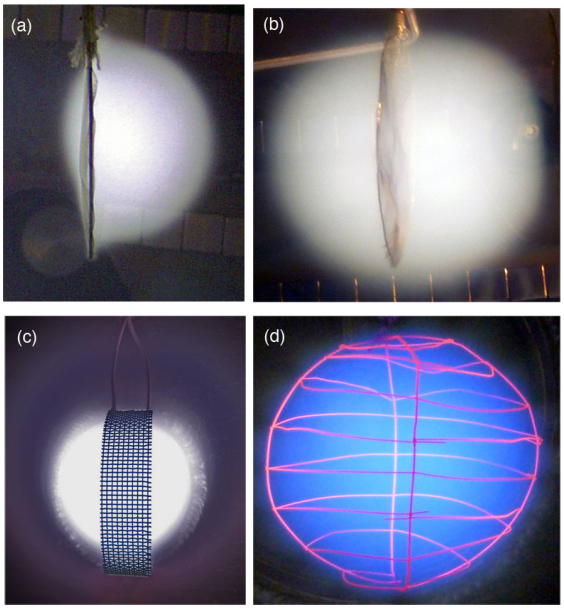

Figure 14: Transition from sheath to fireball on different electrodes. (a) Expanded sheath on a circular plane grid (5 cm diam.). The fireball grows usually on one side of the grid. (b) Increased grid voltage expands the sheath to form a spherical fireball. The sharp light boundary indicates a double layer, i.e., a strong electric field which energizes electrons. (c) A short cylindrical electrode forms a fireball inside the circular grid, the first step to confine the fireball. (d) An "inverted" fireball forms inside a spherical grid with mesh of high transparency. The wire mesh is biased positively which forms an electron-rich sheath. The energized electrons inside the sphere ionize and excite blue light indicating that electrons are energized well above the ionization energy. Figure reprinted from reference [16].

fireball size and location are fixed by the spherical grid, second the double layer is formed at the grid where ions are ejected outward and electrons are accelerated inward. The potential drop can be well above the ionization potential. Trapped fireballs can be formed at low neutral pressures.

Fireballs have several types of instabilities. Low frequency relaxation instabilities arise when production and losses are unbalanced. Electron transit times through the sphere can produce oscillations. Finally the sheath-plasma resonance at the electrode can be destabilized. These will be described below.

X.a) Relaxation instabilities of fireballs

The stability of a fireball requires balance between plasma production and losses, otherwise the location and size of the double layer and its potential drop are not constant. The relaxation oscillations are the dominant instabilities of fireballs. Other in-

stabilities are due to the high-frequency oscillation of the electron sheath-plasma resonance, transit transit time oscillations in inverted fireballs and finally ionization inside sheaths which produces strong sheath perturbations.

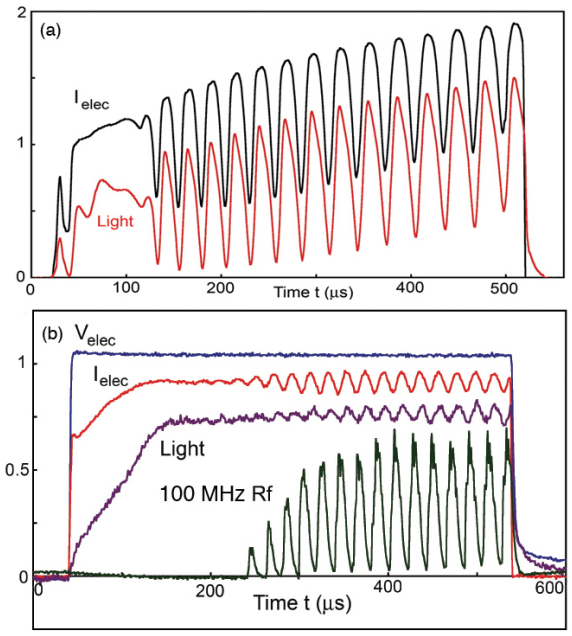

Figure 15: Relaxation oscillations of an unstable fireball. (a) The electrode voltage is switched on so as to observe growth and decay of the fireball. The instability starts upon growth of the fireball. Electrode current and light emission are correlated. The relaxation period is approximately the ion transit time through the fireball which also indicates the ion loss. With gradually increasing current and light the fireballs grow and the repetition time increases. (b) A fireball with small relaxation oscillation in electrode current and light at a low electrode voltage. The amplitude of the high frequency sheath plasma instability is strongly modulated. Figure reprinted from reference [17].

When the fireball is not in equilibrium it gives rise to relaxation oscillations. By pulsing the electrode voltage the growth and decay of the relaxation instability can be seen [17]. Figure 15 (a) shows the electrode current and light emission which correlate and indicate the strength of the fireball. After the initial formation of a fireball the oscillations grow and vanish instantly when $V_{elec} = 0$. The relaxation period corresponds to the ion transit time out of the fireball [5 cm/(2×10^{5}cm/s) = 25 μs]. The relaxation time increases slightly as the fireball size increases.

In order to produce plasma the fireball potential has to exceed the ionization potential. The fireball discharge has a hysteresis for the current turn-on and off. When the external current circuit has an series resistance and capacitance the relaxation instability occurs similar to the well-known Neon R-C oscillator [37]. Fireballs vary in size and light intensity with electron currents. Thus time-averaged light images produce fuzzy boundaries for unstable fireballs and while stable fireballs have sharp discontinuities. In addition to the low frequency relaxation instability there is also the electron sheath-plasma instability at the electrode. Figure 15 (b) shows a fireball with a weak relaxation amplitude and a 100 MHz sheath-plasma instability amplitude which is modulated by the fireball relaxation. The rf amplitude and frequency is highly sensitive to sheath perturbations.

XI. Inverted fireballs with transit time instabilities

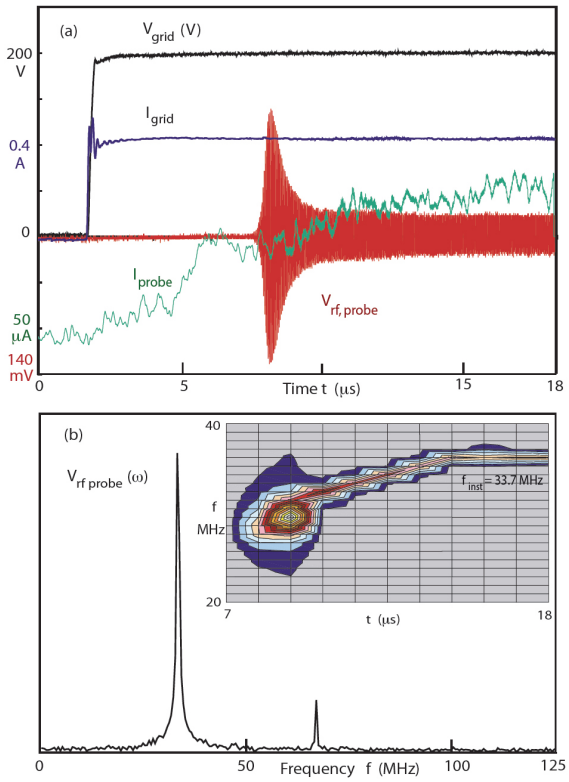

Figure 16: (a) An inverted fireball produces a new instability which involves the electron transit time through the sphere. Grid voltage and current remain constant after turn on. The density inside the sphere shows a gradual increase. The instability has a threshold, followed by an overshoot and constant amplitude. (b) Spectrum of the instability shows a sharp line (35 MHz) whose period is comparable to the electron transit time through the sphere [10 cm/(3×10^8 cm/s)=33 ns]. The instability frequency increases gradually with density. Figures reprinted from reference [38].

A spherical wire mesh of high transparency

is biased positively and surrounded by an ambient discharge plasma. The ambient ions are repelled by the grid while the ambient primary and secondary electrons enter the sphere. An inverted fireball is formed by ionization inside the sphere. At low neutral gas pressure (0.05 Pa) the fireball color is blue, indicating electron energy of order of the applied grid voltage [Fig. 14 (d)] . When the neutral density is increased the color changes to white indicating electrons with lower energy ($\simeq$ 15 eV) as in regular fireballs [Fig. 14 (b)] .

By applying a step-function grid voltage the constant grid current is observed, but the density inside the sphere ($n_e \propto I_{ion,sat}$) grows slowly. After the fireball has grown an instability is seen with an rf oscillation of f $\simeq$ 30 MHz whose period is the electron transit time through the sphere. Figure 16 (b) shows the instability in the frequency domain. The spectral line falls between ion and electron plasma frequencies where propagating waves are evanescent. It is a transit time instability whose period corresponds to the electron transit time across the sphere. Electron bunches travel from sheath to sheath. When they are delayed by one rf period with respect to an ac sheath electric field the field-particle interaction leads to a positive feedback similar to transit time instabilities in real and virtual sheaths. The frequency depends on the size of the sphere, verified with different spheres, and the electron velocity which is controlled by the grid voltage. By pulsing the grid voltage the plasma density grows slowly, the instability starts with an overshoot and continues to rise in density, plasma frequency and instability frequency.

The fundamental mode of the transit time instability is a radial standing wave has a half wavelength diametrically, a second mode has a full wavelength of one diameter, etc., [38, 39]. The modes are not harmonics due to nonlinearities but independent eigenmodes. With a resonant circuit in series with the grid the individual modes can be tuned out without affecting other spectral lines. Since the grid is biased highly positive the ambient plasma ions are repelled by the sphere. Ions are produced by ionization inside the sphere. In steady state the ion production must be balanced by ion losses. Ions leave the sphere when the interior plasma potential is slightly above the grid potential. Electrons are collected by the grid wire from both sides causing the wire to glow red . Between the grid wires the potential is again a double layer, electron-rich outside the grid, ion rich inside the grid.

XII. Inverted fireballs with secondary electron emission

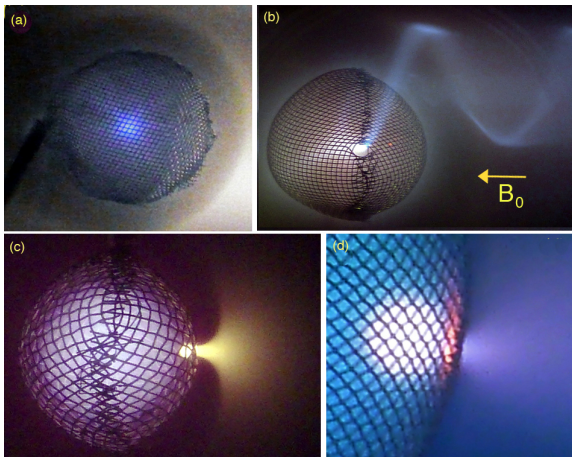

Figure 17: Spherical grids for studying inverse fireballs. (a) Gridded sphere with strong negative bias (-500 V) producing a thick ion rich sheath in an ambient dc discharge. The light arises from secondary electron emission by ion impact with the grid. Electrons and ions focus at the center of the sphere producing light. (b) A small hole in the grid allows electrons to leave as a beam. In a uniform magnetic field the pitch angle and cyclotron radius yield the beam energy and plasma potential in the sphere (-250 V). (c) Increasing the neutral pressure a firerod is formed in the hole ($\mathbf{B}_0 = 0$). The light indicates that the firerod acts like an anode to the plasma inside the sphere. (d) Further increase of neutrals forms a small spherical fireball *inside* the sphere. The potential inside the sphere differs only by the ionization potential from the fireball or ambient plasma. The injected ions have insufficient energy to produce secondary electron emission. Thus energetic ambient electrons enter via the fireball into the sphere which fills the sphere with plasma.

In a normal or inverted fireball the grid bias is positive so that electrons are injected into the fireball. Ions are normally produced by ionization inside the grid. However, without ionization a plasma in a sphere can also be accomplished by injecting energetic ions which produce secondary electrons from the inner grid. Pictures of inverse fireballs with negative grid bias are shown in Figs. 17. With a gridded wire mesh a light emission is observed in the center of the sphere where the injected electrons focus. Such a confinement has been proposed to focus ions for an inertial fusion device ("fusor") [33] but that is not the present objective.Figure 17 (a) shows a completely closed grid biased at $V_{grid} = -500$ V. The light is due to electron-neutral excitation, thus is a measure of the electron density and energy. It peaks in the center. Ions are not visible but evident from

the grid current. The ambient plasma is hardly visible. A dark shadow forms around the outer grid which is the ion-rich sheath due to the high bias voltage. In order to insert a diagnostic probe into the sphere a small hole has been formed in the wire mesh. Before inserting a probe the electrons escaped from the small hole. The electrons form a visible beam shown in Fig. 17 (b). By applying a weak magnetic field the beam energy is found from the cyclotron radius and pitch angle.

The beam originates from the plasma near the hole in the grid, hence it shows that the plasma potential inside the sphere is negative relative to the ambient plasma potential near ground. Near the hole the equipotential contours penetrate into the grid opening. The electron acceleration starts already inside the sphere [Fig. 17 (c)]. At higher neutral pressures a spherical fireball forms *inside* the sphere [Fig. 17 (d)]. The sharp light boundary is again the location of a double layer or an equipotential contour. The fireball acts like the positive anode collecting electrons from inside the sphere. Outside the grid the beam spreads due to a radial space charge electric field. Since the double layer potential is of the order of the ionization potential ($\propto$ 15 eV in Ar) the interior plasma potential must be 15 V lower than the ambient plasma potential. The highly negative grid potential forms a localized sheath near the grid. Ionization is the dominant ion source. Ions gain energy in the grid sheath and still produce secondary electrons. The secondary electrons gain energy from the potential drop between the sheath and the interior of the grid where light and ionization dominate. The interior forms a dc discharge where the grid is the cathode and the fireball is the anode. This holds also for the ambient plasma where the sphere is an ion collector (anode) and the fireball emits electrons (cathode). The fireball size, potential and density control the balance of electron and ion flows.

XIII. Sheaths and instabilities for plasma confinement

Plasma can be produced by ionization or by adding ions and electrons from separate sources. The latter method is shown for a spherical mesh grid [40]. When the grid is biased negatively the ions from the ambient plasma are injected into the sphere. If the ions have too little energy they produce no ion-neutral collisions and no secondary electrons by impact on the grid. Without electron sources the injected ions form a space charge layer just inside the grid (a "virtual anode") which reflects all ions and leaves a vacuum inside the sphere (a plasma "bubble"). In order to produce a plasma inside the grid one has to insert a cathode which emits electrons to neutralize the ion space charge.

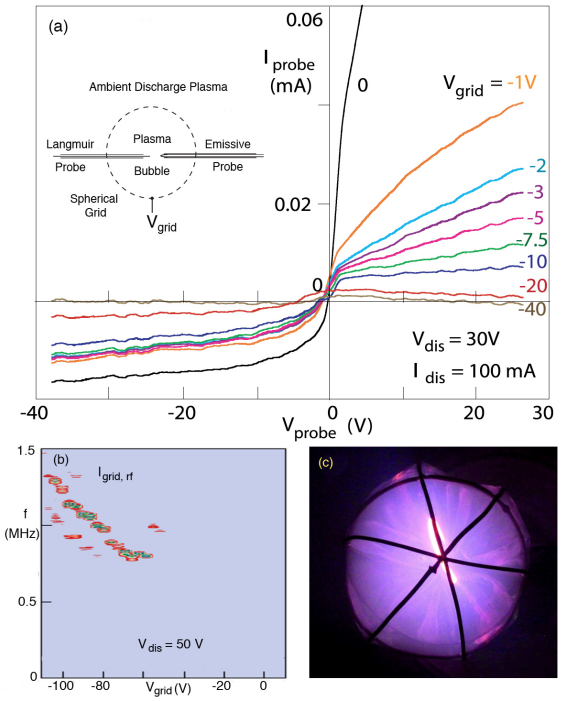

Figure 18: (a) Langmuir probe characteristics inside a gridded sphere (see insert). The grid voltage is increased from zero to beyond the discharge voltage of the ambient dc discharge. For $|V_{grid}| > V_{dis}$ the electrons are repelled at the outer sheath and the attracted ions form a virtual anode just inside of the grid. The sphere is a plasma bubble. (b) Instability of the virtual anode. Its frequency is governed by the ion transit time through the ion sheath. The frequency decreases with increasing sheath thickness controlled by $|V_{grid}|$. (c) The image displays electrostatic confinement of plasma. The electrons are emitted from a hot cathode and are reflected by a large negative bias. Ions cannot expand beyond the grid without electrons, hence reflects by forming a virtual anode. Figures reprinted from reference [40].

We demonstrate the formation of a bubble using a gridded sphere surrounded by an ambient discharge plasma. A cathode is inserted but is cold and not yet emitting. The grid current vs grid voltage is shown in Fig. 18 (a). For low grid voltages the ambient electrons and ions leak into the sphere similar to the external plasma. When the negative grid voltage just exceeds the energy of the primary electrons of the ambient discharge (50 V) the electron and ion currents are equal and cancel, i.e., the grid is floating. With further grid bias all electrons are repelled, all ions are reflected by a virtual anode at the inside of the grid. No plasma is in the sphere, i.e., it is a bubble. Virtual anodes and cathodes are unstable due to a time delay of

particles relative to sheath electric field oscillations. The transit time instability for electrons arises when the cathodes emits into vacuum forming a virtual cathode ("vircator"). Related transit time effects cause an rf instability at the sheath-plasma resonance (see Section II). The travel time through the sheath determines the instability frequency which is below the electron plasma frequency. Figure 18 (b) shows the spectrum of the virtual anode instability. When the grid voltage exceeds the energy of the external primary electrons ($|V_{grid}| > |V_{dis}|$) a virtual anode is formed in the bubble. The oscillation is observed on the grid but not in the empty bubble with probes. The instability frequency is in the range of the ion plasma frequency. The frequency decreases with grid voltage which widens the sheath and increases the ion transit time. When the grid voltage is smaller than the discharge voltage the ambient electrons neutralize the virtual anode, fills the sphere with plasma and the transit time instability vanishes.

When an emissive cathode is inserted into the sphere the reverse location of a potential similar to a virtual cathode can be formed [40]. Figure 18 (c) shows the cathode producing a discharge plasma within the spherical grid. In contrast to solid anodes the grid is highly transparent, which can transmit, reflect and collect particles. The spherical grid is surrounded by an ambient discharge plasma which is pulsed. The discharge has primary and secondary electrons, but the energetic electrons can be removed by using the Maxwellian afterglow plasma with cold electrons and decreasing density. The light emission is produced by inelastic electron collisions ($kT_e > 15$ eV) with neutrals. The weak ambient discharge produces negligible light, but the plasma in the sphere is bright when the grid is negative. When the cathode inside the sphere is cold and not emitting, only ions from the ambient plasma are attracted by the negative grid bias, say $V_{grid} = -80$ V. All electrons are repelled, both low energy discharge electrons and high energy primary electrons ($V_{dis} = -50$ V). The lack of electrons stops the inflow of ions which leads to a virtual anode just inside the grid. The bubble contains no plasma. In order to emit electrons the cathode has to be hot and biased negative relative to the plasma potential. In the absence of an ambient plasma the cathode does not emit electrons into vacuum, provided the cathode voltage is positive with respect to the grid. On the other hand when the cathode voltage is biased more negative than the grid voltage a small current is observed to flow [40]. This is due to ionization inside the sphere which requires a plasma potential above the cathode potential by at least the ionization potential. When the plasma potential is below the grid potential the ions cannot escape from the sphere. The electrons could escape but not without ions. Thus, just outside the grid a space charge layer builds up to reflect the electrons most of which are collected by the grid anode. The trapped electrons excite light with neutrals. The electron energy for excitation and ionization are comparable (10-20 eV). Since there is no light outside the sphere the plasma is confined inside the sphere.

In steady state the electron and ion fluxes have to be balanced which is accomplished by the sheath and plasma potential. The ions are collected by the negative cathode, the electrons are collected by the grid. Inserting biased probes can change the particle fluxes and potentials. An ambient plasma alters the spherical plasma due to ion injection and losses. No ambient plasma is needed since ionization supplies the plasma. Double plasma devices have been used extensively to excite beams and waves [41]. The confinement of a spherical plasma has not yet been used as an efficient plasma source. By pulsing the spherical plasma the measured decay time is $\tau \simeq 100$ μs while the time of flight of ions at the sound speed through the sphere is 4 cm/4$\times 10^5$ cm/s = 10 μs. Electrostatic confinement is not perfect, but magnetic confinement is neither ideal. The sheath around the grid is rich in oscillations. For example, a low frequency instability arises from a virtual anode-like sheath which reflects the ions. The frequency is below the ion plasma frequency and has copious harmonics and subharmonics. When electrons enter into the virtual anode the virtual anode instability disappears.

XIV. Magnetron plasmas

Magnetrons are used for microwave oscillators and plasma sources for sputtering. The basic principle is a circular electron layer which performs an $\mathbf{E}\times\mathbf{B}_0$ drift past several resonant cavities. Electron bunches travel and reinforce the cavity electric field which results in an oscillation or instability.

In the present work a permanent magnet is immersed into an ambient unmagnetized plasma source. The shape of magnets can be spherical, cylindrical and long bars. Figure 19 (a) shows a strong Neodymium (Nd, 5 kG) ball magnet (5 cm diam.) which is biased negatively. To recall the particle movement in a dipole field a small emissive filament emits test electrons. They travel along the magnetic field lines, reflect by magnetic mirror-

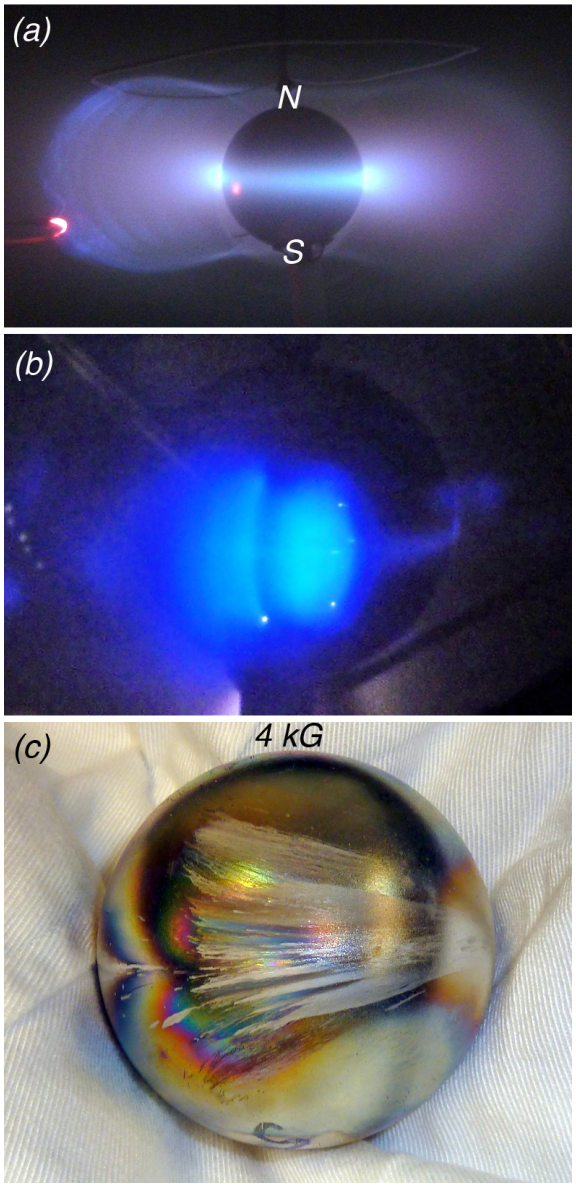

Figure 19: Test wave and sheath ionization on a permanent magnet biased negatively. (a) A 5 cm diam. neodymium ball magnet biased at -400 V. A small emissive probe emits 100 eV electrons to show the particle motion in a dipole field: Cyclotron orbits, guiding center drifts due to magnetic field gradient, field line curvature and $\mathbf{E} \times \mathbf{B}$ drift. At the equator a bright ring of plasma is formed by ion impact creating secondary electron emission. (b) Spot discharges (see white spots) produce plasma near the equator and broad discharge streaks to the wall to satisfy current closure. (c) The magnet surface eroding due to ion impact and spot arcs. The streaks propagate along the equator due to particle drifts. Streaks expand toward the poles since with increasing height the plasma flux tubes impact away from the equator. Figures reprinted from reference [28].

ing or the sheath at the magnet, drift azimuthally around the magnet axis due to the magnetic gradient and field line curvature. At a pressure of 100...1000 Pa electron-neutral collisions diffuse the initially discrete particle motions. When the conducting magnet is biased highly negative (-500 V) the impact of energetic ions on the magnet causes secondary electron emission. The emitted electrons perform both an $\mathbf{E}\times\mathbf{B}$ drift and the magnetic gradient and curvature drifts. Near the equator the drift is parallel to the surface, the electrons have a long time to ionize and excite the gas which is the reason for the bright equatorial plasma ring. In the equatorial region the potential is negative and the density peaks. The magnet is pulsed and its afterglow replaces the need for an ambient plasma since steady-state operation would overheat the magnet and demagnetize it [28, 29]. Note that in Fig. 10 (a) an electron drift is produces differently: The spherical electrode is not a magnet, it is biased positively, the ambient magnetic field is horizontal and uniform hence no magnetic drifts arise. A plasma layer forms on the surface of the ball electrode where the $\mathbf{E} \times \mathbf{B}_0$ drift maximizes, hence electrons have the longest lifetime.

XV. Sputtering and Coating

When the negative bias voltage on the magnet is increased random flashes arise. Figure 19 (b) shows small bright spots create localized plasma clouds near the magnet equator. Since a camera cannot resolve microsecond events multiple spots may be sequential ones. The spots are random in position and time and produce large, short but high current pulses (500 A at -700 V). The bright spots are thought to be melt-down of the magnet material which produces dense plasmas carrying high currents. Figure 19 (c) shows the pitted magnet surface. The streaks indicate drifts in equatorial and polar directions and short lifetime [28, 29].

Figure 20 (a) shows that with increasing voltage the current to the magnet rises exponentially since the secondary electron emission goes over into an arc mode [29]. In order to avoid heating and demagnetizing the permanent magnet one has use pulsed voltages with low duty cycle due to the high power levels (800 V, 100 A, 80 kW). Unfortunately, the diagnostics of arc discharges is difficult since the spot arcs are irreproducible in location and time [see Fig. 20(b)]. Arc discharges arise from melting the surface material which produces high plasma densities and large currents of short rise times (500 A/μs). Figure 20 (c) shows expanded waveforms of magnet current and voltage for the first shot. In order to supply large currents a charged capacitor is placed at the vacuum feedthrough to minimize inductive effects (see insert). As the current rises the capacitor

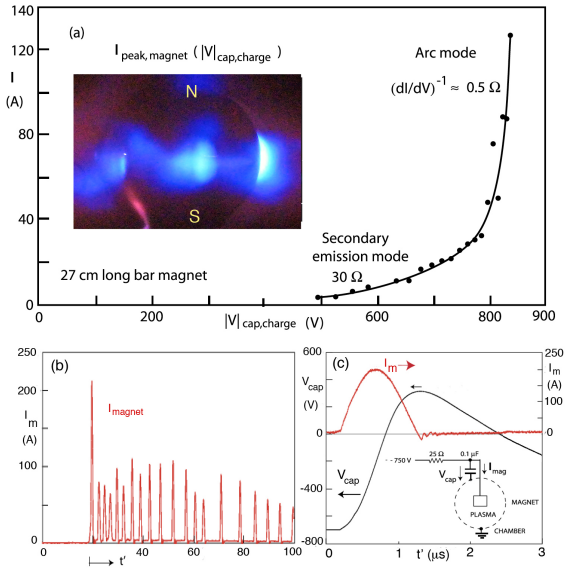

Figure 20: (a) Current-voltage characteristics of a magnetron plasma. At low voltages the plasma is produced by secondary electron emission from ion impact. At higher voltages arc discharges dominate. Insert shows an image of arc discharges. (b) Waveforms of the magnet current for $V_{grid\ dc}$ =-750 V. Spot discharges have positive random pulses. (c) Current and voltage for a single arc pulse on an expanded time scale. Inductive effects reverse the voltage due to circuit capacitance, inductance and resistance. Figures reprinted from reference [29].

voltage decreases, crosses zero and reverses sign when the magnet current vanishes. This is characteristic of an L-C circuit where the inductance is due to the short connection to the magnet and the plasma current closure path from the magnet to the wall. The arcs discharges are electromagnetic phenomena, which include sheaths, plasma and ambient circuit component.

Arcs occur not only on the magnet but also on probes biased to -500 V [see Fig. 21 (a)]. The streaks are ejected cathode material. The arc plasma on a bar magnet has frequently white spots which are the source of the arc [see Fig. 21 (b)]. When the spots move radially away from the equator the plasma broadens since the electrons remain on the dipole field lines. The vertical plasma streaks are ionization phenomena required to carry the return current to the chamber wall. A useful application of sputtering is coating [44]. The simplest setup is to place the material on the equator of the magnet, such as an aluminum sheet metal strip or tungsten wire [Fig. 21 (c,d)]. The material sputters and deposits it near the plasma, for example on the magnets themselves or a nearby ceramic tube. Non-conducting ferrite magnets can easily be changed into conducting magnets. Similarly ceramic tubing can be coated and used for high temperature coaxial conductors [28].

XVI. Neutral gas heating and acceleration from fireballs

The last experiment has potential relevance for thrusters and processing applications [42, 43, 44, 45]. The basic approach is to accelerate ions in electric fields due to double layers or plasma expansion along diverging magnetic fields. However, heating neutrals can also exert forces. It is observed that neutrals are expelled due to pressure gradients and not by potential gradients like ions [46]. Neutral ejection can also be detrimental in helicon devices where a burn-out of neutrals can disrupt the discharge [47, 48].

The first observation was that a fireball on a movable electrode causes a recoil motion [46]. The effect is enhanced when the electrode is suspended like a pendulum and the fireball is pulsed at the frequency of the pendulum [Fig. 22 (a,b)]. Alternatively the fireball electrode is fixed and a small mica sheet is suspended at a short distance from the fireball [Fig. 23 (a, insert)]. The deflection is measured with a laser beam which reflects from the mica surface. It is detected with two photodiodes which convert the light into electrical pulses when the reflected beam sweeps over the diodes. This method is sensitive and detects small pendulum deflections. The deflection does not arise from charged particles since a conducting sensor has been biased without response. For possible applications it would be desirably to obtain a collimated beam. By inserting a disc electrode in a pyrex glass tube the discharge becomes cylindrical but mostly ends with a spherical fireball. When the gas pressure is reduced a cylindrical firerod is formed without magnetic field. With high electrode bias and moderate gas pressure the cylindrical discharge becomes a jet beyond the tube. The velocity of the gas jet has been measured as described in Fig. 23 (a). From the displacement and time of the light beam one obtains the velocity of the mica sensor which is a close estimate of the gas flow since the sensor is light and has little friction. By rotating the jet a polar plot of the gas flow is obtained [Fig. 23 (b)]. The half width is close to 30°. The flow velocity is found to be v_{gas} =37 m/s, the gas pressure is 3×10^{-2} Pa, which is much larger than the plasma pressure of $nkT_e \simeq 3\times10^{-4}$ Pa.

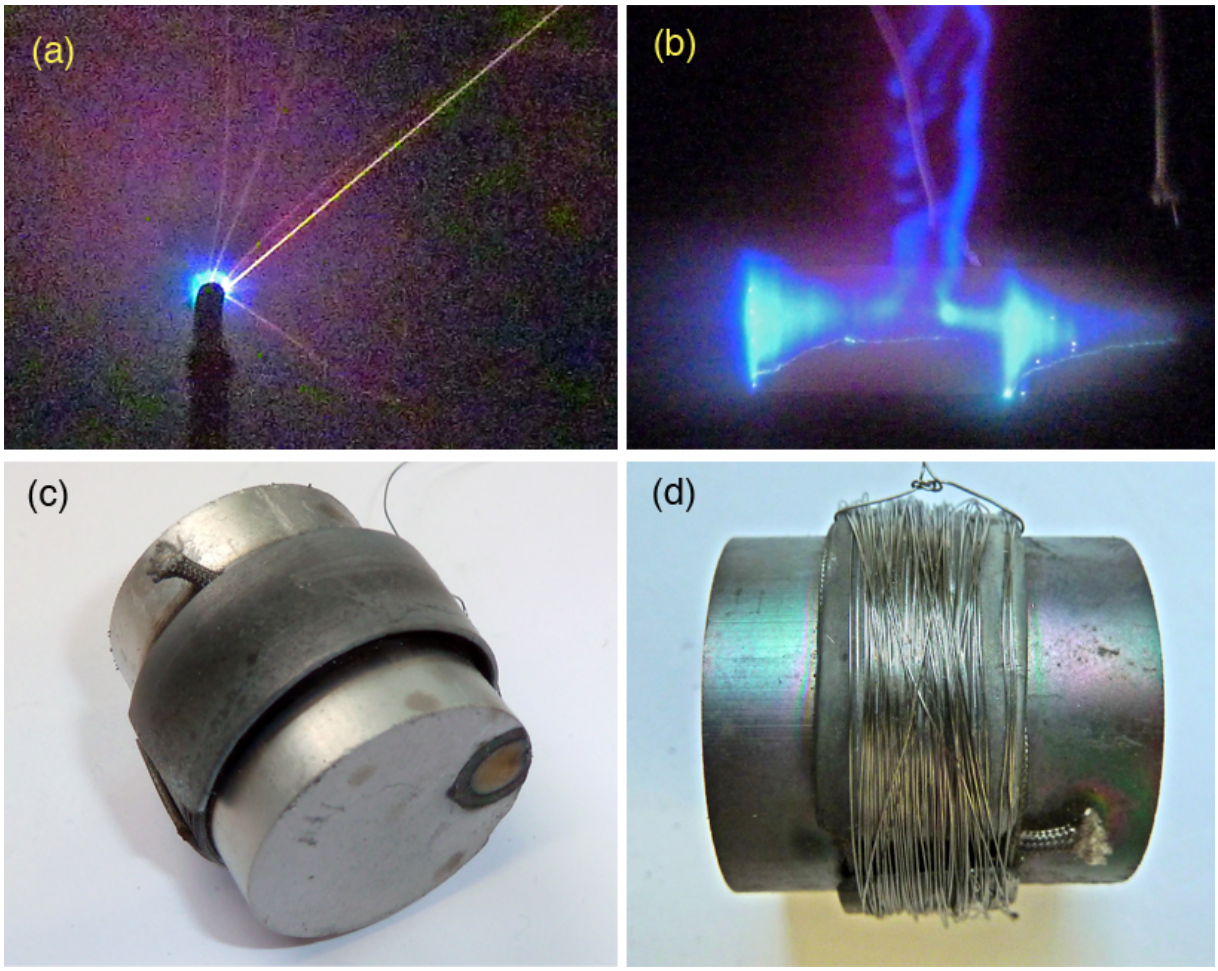

Figure 21: Examples of sputtering and coating. (a) A negatively biased Langmuir probe ejects material due to an arc discharge. (b) Arc plasmas on a bar magnet. White spots or streaks are the source for the plasma. (c) Permanent magnet with a strip of aluminum (Al) metal, biased to -500 V. The magnet is floating and coated with a layer of Al. (d) Coating the magnet with a layer of tungsten (W) which was sputtered from a layer of W wire. Figures reprinted from reference [28, 29].

XVII. Summary

The review shows a large number, but not all sheath phenomena and instabilities. Since sheaths are localized, most instabilities are absolute, while propagating and growing waves usually originate from convective instabilities. Sheaths can also support several instabilities such as transit time instabilities at electron and ion plasma frequencies, interrupted by low frequency spontaneous ionization events. The physics of sheaths is often treated as a local phenomenon, but in reality it is a global plasma system with plasma sources, sinks and boundaries. Sheaths can become easily unstable since they are regions of different charge densities. Several basic phenomena have been pointed out from observations of laboratory experiments: (i) Transit time effects of charged particles in regions of electric fields, for example a sheath plasma resonance. The latter is nonlinear and forms parametric decay and electron and ion oscillations. (ii) Electron drift modes with high mode numbers arise in magnetized electron sheaths. (iii) The modification of sheaths into double sheaths in collisional and collisionless plasmas. The latter arises when ions (electrons) are injected into electron-rich (ion-rich) sheaths. Multiple double layers arise at plasma boundaries. (iv) Ionization in electron-rich sheaths modulates potential profiles and can evolve into double layers of fireballs. Fireballs can heat neutrals and produce gas jets. (v) Electrostatic confinement of plasmas create virtual cathodes and anodes which have transit time instabilities from reflections of electrons or ions. (vi) Secondary emissions arise from energetic electron and ion impacts with solid boundaries. The combination of a sheath with negative resistance and an external resonant circuit results in low frequency oscillations of large amplitudes and rich harmonics. (vii) A positively biased electrode in a weakly magnetized plasma does not only produce an electron rich sheath but also develops perpendicular potential

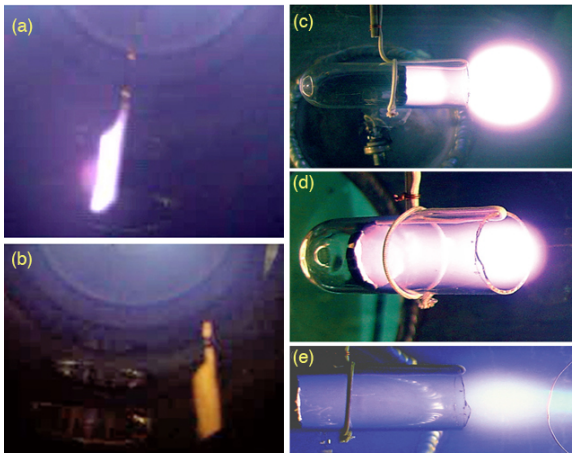

Figure 22: An electrode recoils when a fireball is excited. The plane probe is conducting on one side. It is suspended on a pendulum and pulsed with its resonant frequency. The fireball starts to swing and reaches large excursions [(a) to (b)] with a small resonant driving force. The force arises from heated neutral gas pushed away from the electrode. In order to obtain a more collimated gas flow the electrode is inserted into a pyrex tube. (c) At high neutral pressure the fireball forms at the end of the tube. (d) At decreasing electrode bias the fireball shrinks into the tube. (e) At low gas pressure and high bias and retracted electrode results in a jet-like fireball. Note that a floating wire begins to glow which is an indication of the high gas temperature. Figures reprinted from reference [46].

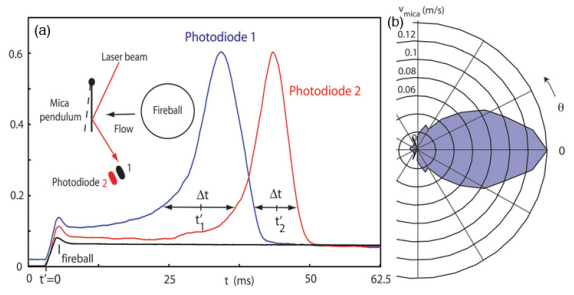

Figure 23: (a) Quantitative measurement of the gas velocity. The fireball is stationary and a torsional mica sheet is the sensor. A laser beam reflects and magnifies the displacement measured externally. From displacement and time the velocity is obtained. (b) Polar plot of the sensor velocity which has very small friction, hence is a measure of the gas velocity. Forces of ions or electrons are negligible since a conducting sensor does not respond to the sensor bias. Figures reprinted from reference [46].

drops which accelerate ions in and out of the flux tube. The density disruptions produce current pulses with repetition at the ion transit time across the flux tube. (viii) Fast current pulses are not only governed by sheath properties but also by propagating electromagnetic phenomena. Pulsed currents travel as vortices in the whistler mode. Current pulses are not predicted by Langmuir probe theory but have to investigate current transport by waves. In magnetic reconnection localized currents can produce density depletions, large inductive electric fields and strong collisionless double layers without ionization.

Many of the experimental observations deserve more theories. Many experiments should measure velocity distribution functions to address kinetic instabilities and anomalous transport. The diagnostic tools exist and some examples have demonstrated distribution functions in 3D velocity space, real space and time [49, 50], but little is known of distributions near sheaths. The heat transport from plasma to neutrals deserves further investigations for gas flow applications [46]. The research on sheaths, instabilities and global effects should be advanced and extended to applications such as plasma propulsion [42], plasma processing [43] and depositions [44] and plasma medicine [51]. The research on sheaths can also have applications in industry, medicine and defense, for example isotope separation. It has been shown that a positively biased electrode raises the plasma potential in the flux tube of the electrode, i.e., a perpendicular electric field. By modifying the electrode into segmented rings with different bias a radial electric field penetrates throughout the plasma. When the bias is oscillating at the ion cyclotron frequency the ions and its isotopes are resonantly energized and the large orbit ions are deposited with suitable collectors [52, 53].

There are also many problems in space plasmas where sheath physics is important [54, 55]. For example, electrodynamic tethers are useful to generate energy, propel spacecraft, radiate waves, etc. The tether consists of a long (20 km) wire with electron collector and emitter at the ends, which flies across the Earth's magnetic field and induces high voltages and significant currents. The sheaths cannot be treated without considering the current system. Although the current in the tether is a dc current the current in the plasma is a time-varying pulse whose duration is the transit time of the electrode and the satellite speed. The repeated current pulses join into a tilted "whistler wing" like a Cerenkov wing. Laboratory experiments show that the current closure forms a whistler wing of twisted current tubes and a cross-field Hall current radiated from a linear antenna [56]. Since the current overshoot exceeded the electron saturation current the tether current exceeded the steady state theory [25]. An experiment in space failed since the tether melted. In space it is difficult to diagnose the complex interrelation between electrodes, sheaths and

wave currents. Another application of Hall physics deals with the problem of sheaths for reentrant hypersonic vehicles. A plasma layer is formed by impact ionization and causes communication blackout which needs to be removed. Based on observations in the laboratory that ions can be expelled by Hall electric fields it is predicted that plasma from the vehicle surface can be removed [57].

XVIII. Acknowledgments

The different experiments have been performed with many collaborators at different times and locations. Great appreciation are for collaborations during invited sabbatical in Tokyo by Yoshi Nakamura, frequent sabbaticals at the University of Innsbruck with the group of Roman Schrittwieser, especially with Codrina Ionita and Johannes Gruenwald, and my collaborators and students at the University of California Los Angeles, particularly by Manuel Urrutia. I specially thank Johannes Gruenwald for suggesting this review. The authors also acknowledge the reviewers effort to carefully read the long review manuscript . The support for the many research projects was funded by the University of Tokyo, the Austrian Science Fund at the University of Innsbruck, and in the United States by the National Science Foundation.

XIX. References

[1] I. Langmuir, "Positive Ion Currents from the Positive Column of Mercury Arcs," *Science*, vol. 58, no. 1502, p. 290, 1923. https://doi.org/10.1126/science.58.1502.290

[2] F. B. Llewellyn, and L.C. Peterson, "Vacuum-Tube Networks," *Proceedings of the IRE*, vol. 32, no. 3, p. 144, 1944. https://doi.org/10.1109/jrproc.1944.230037

[3] R. S. Harp, and F. W. Crawford, "Characteristics of the Plasma Resonance Probe," *J. Appl. Phys.*, vol. 35, no. 12, p. 3436, 1964. https://doi.org/10.1063/1.1713246

[4] R. L. Stenzel, "High-frequency instability of the sheath-plasma resonance," *Phys. Fluids B*, vol. 1, no. 11, p. 2273, 1989. https://doi.org/10.1063/1.859042

[5] Yu. P. Bliokh, J. Feltsteiner, and Ya. Z. Slutsker, "Existence and stability of the plasma sheath resonance near the ion plasma frequency," *EPL (Europhys. Lett.),*, vol. 46, no. 6, p. 735, 1999. https://dx.doi.org/10.1209/epl/i1999-00326-y

[6] R. L. Stenzel, H. C. Kim, and A. Y. Wong, "Parametric Instability of the Sheath-Plasma Resonance," *Radio Science*, vol. 10, no. 4, p. 485, 1974. https://doi.org/10.1029/rs010i004p00485

[7] M. C. Griskey, and R. L. Stenzel, "Secondary-electron-emission instability in a plasma," *Phys. Rev. Lett.*, vol. 82, no. 3, p. 556, 1999. https://doi.org/10.1103/physrevlett.82.556

[8] Y. Nakamura, Y. Nomura, and R. L. Stenzel, "Sheath expansion of plane probe by ion-beam reflection," *J. Appl. Phys.*, vol. 52, no. 3, p. 1197, 1981. https://doi.org/10.1063/1.329737

[9] R. L. Stenzel, M. Ooyama, and Y. Nakamura, "Potential double layers formed by ion beam reflection in magnetized plasmas ," *Phys. Fluids*, vol. 24, no. 4, p. 708, 1981. https://doi.org/10.1063/1.863435

[10] G. Hairapetian, and R. L. Stenzel, "Particle dynamics and current-free double layers in an expanding, collisionless two-electron-population plasma," *Phys. Fluids B*, vol. 3, no. 4, p. 899, 1991. https://doi.org/10.1063/1.859847

[11] R. L. Stenzel, and G. Hairapetian, "Current-Free Double Layer in an Expanding Plasma with two Electron Populations," *Symposium on Double Layers and Other Nonlinear Potential Structures in Plasmas, Innsbruck, Austria, July 6-8, 1992, R. W. Schrittwieser, editor (World Scientific, Singapore)*, p. 291, (1993), 1991. https://doi.org/10.1142/9789814535656

[12] "R. L. Stenzel, J. Gruenwald, C. Ionita, and R. Schrittwieser, "Electron-rich sheath dynamics. II. Sheath ionization and relaxation instabilities", *Phys. Plasmas*, vol. 18, no. 6, p. 062113, 2011. https://dx.doi.org/10.1063/1.3601860

[13] T. An, R. L. Merlino, and N. D'Angelo, "Cylindrical Anode Double Layers, Firerods Produced in a Uniform Magnetic Field," *J. Phys. D: Appl. Phys.*, vol. 27, no. 9, p. 1906, 1994. https://doi.org/10.1088/0022-3727/27/9/014

[14] V. Pohoata, G. Popa, R. Schrittwieser, C. Ionita, and M. Cercek, "Properties and control of anode double layer oscillations and related phenomena," *Phys. Rev. E*, vol. 68, no. 3, p. 016405, 2003. https://doi.org/10.1103/physreve.68.016405

[15] D. G. Dimitriu, M. Aflori, L. Ivan, C. Ionita, and R. Schrittwieser, "Common physical mechanism for concentric and non-concentric

multiple double layers in plasma," *Plasma Phys. Contr. F.*, vol. 49, no. 3, pp. 237–248, 2007. https://dx.doi.org/10.1088/0741-3335/49/3/004

[16] R. L. Stenzel, J. Gruenwald, C. Ionita, and R. Schrittwieser, "Pulsed, unstable and magnetized fireballs," *Plasma Sources Sci. Technol.*, vol. 21, no. 1, p. 015012, 2012. https://dx.doi.org/10.1088/0963-0252/21/1/015012

[17] R. L. Stenzel, C. Ionita, and R. Schrittwieser, "Dynamics of fireballs," *Plasma Sources Sci. Technol.*, vol. 17, no. 3, p. 035006, 2008. https://dx.doi.org/10.1088/0963-0252/17/3/035006

[18] S. D. Baalrud, B. Scheiner, B. Yee, M. M. Hopkins, and E. Barnat, "Interaction of biased electrodes and plasmas: Sheaths, double layers and fireballs," *Plasma Sources Sci. Technol.*, vol. 29, no. 5, p. 053001, 2020. https://dx.doi.org/10.1088/1361-6595/ab8177

[19] R. L. Stenzel, J. M. Urrutia, C. Ionita, and R. Schrittwieser, "High frequency instability of a magnetized spherical electron sheath," *Phys. Plasmas*, vol. 17, no. 6, p. 062109, 2010. https://dx.doi.org/10.1063/1.3437398

[20] R. L. Stenzel, J. Gruenwald, B. Fonda, C. Ionita, and R. Schrittwieser, "High frequency instabilities in an inverted fireball. I. Basic properties," *Phys. Plasmas*, vol. 18, p. 012104, 2011. https://dx.doi.org/10.1063/1.3533437

[21] R. L. Stenzel, J. Gruenwald, B. Fonda, C. Ionita, and R. Schrittwieser, " Transit time instabilities in an inverted fireball. I. Basic properties," *Phys. Plasmas*, vol. 18, no. 1, p. 012104, 2011. https://doi.org/10.1063/1.3533437

[22] R. L. Stenzel, J. Gruenwald, B. Fonda, C. Ionita, and R. Schrittwieser, " Transit time instabilities in an inverted fireball. II. Mode jumping and nonlinearities," *Phys. Plasmas*, vol. 18, no. 1, p. 012105, 2011. https://doi.org/10.1063/1.3533440

[23] R. L. Stenzel, J. M. Urrutia, C. T. Teodorescu-Soare, C. Ionita, and R. Schrittwieser, "Magnetic Dipole Discharges. 1. Basic Properties," *Phys. Plasmas* vol. 20, no. 8, p. 083503, 2013. https://dx.doi.org/10.1063/1.4817014

[24] R. L. Stenzel, J. M. Urrutia, C. Ionita, and R. Schrittwieser, "Magnetic Dipole Discharges. 2. Cathode and Anode Spot Discharges and Probe Diagnostics," *Phys. Plasmas* vol. 20, no. 8, p. 083504, 2013. https://doi.org/10.1063/1.4817015

[25] R. L. Stenzel, and J. M. Urrutia, "Pulsed currents carried by whistlers. VIII. Electrode current disruptions by Plasma Erosion," *Phys. Plasmas*, vol. 4, no. 1, p. 26, 1997. https://doi.org/10.1063/1.872109

[26] R. L. Stenzel, W. Gekelman, and N. Wild, "Magnetic Field Line Reconnection Experiments 5. Current Disruptions and Double Layers," *J. Geophys. Res*, vol. 88, no. A6, p. 4793, 1983. https://doi.org/10.1029/ja088ia06p04793

[27] R. L. Hirsch, "Inertial-Electrostatic Confinement of Ionized Fusion Gases," *J. Appl. Phys.*, vol. 38, no. 7, p. 4522, 1967. https://doi.org/10.1063/1.1709162

[28] R. L. Stenzel, J. M. Urrutia, C. T. Teodorescu-Soare, C. Ionita, and R. Schrittwieser, "Magnetic Dipole Discharges. 1. Basic Properties," *Phys. Plasmas* vol. 20, no. 8, p. 083503, 2013. https://dx.doi.org/10.1063/1.4817014

[29] R. L. Stenzel, J. M. Urrutia, C. Ionita, and R. Schrittwieser, "Magnetic Dipole Discharges. 2. Cathode and Anode Spot Discharges and Probe Diagnostics," *Phys. Plasmas* vol. 20, no. 8, p. 083504, 2013. https://doi.org/10.1063/1.4817015

[30] M. Rader, F. Dyer and I. Alexeff, "Electron density and temperature in the pulsed-orbitron-maser glow discharge," *IEEE Trans. Plasma Sci.*, vol. 16, no. 2, p. 270, 1988. https://doi.org/10.1109/27.3824

[31] P. J. Barrett, and R. G. Greaves, "Double-plasma instability near the ion plasma frequency," *Phys. Fluids*, vol. 1, no. 9, p. 1776, 1989. https://dx.doi.org/10.1063/1.858907

[32] C. Charles, "A review of recent laboratory double layer experiments," *Plasma Sources Sci Technol.*, vol. 16, no. 4, p. R1, 2007. https://dx.doi.org/10.1088/0963-0252/16/4/R01

[33] G. H. Miley, et al, "Discharge characteristics of the spherical inertial electrostatic confinement (IEC) device," *IEEE Trans. Plasma Sci.*, vol. 25, no. 4, p. 733, 1997. https://doi.org/10.1109/27.640696

[34] J. M. Urrutia and R. L. Stenzel, "Pulsed currents carried by whistlers. IX. In situ measurements of currents disrupted by plasma erosion," *Phys. Plasmas*, vol. 4, no. 1, p. 36, 1997. https://dx.doi.org/10.1063/1.872492

[35] J. M. Urrutia, and R. L. Stenzel, "Transport of Current by Whistler Waves," *Phys. Rev. Lett.*, vol. 62, no. 2, p. 272, 1988. https://doi.org/10.1103/physrevlett.62.272

[36] R. L. Stenzel, "Whistler modes excited by magnetic antennas: A review," *Phys. Plasmas,* vol. 26, no. 8, p. 080501, 2019. https://doi.org/10.1063/1.5097852

[37] S. O. Pearson, and H. St. G. Anson, "Demonstration of Some Electrical Properties of Neon-filled Lamps," *Proc. Of the Physics Soc. London*, vol. 34, no. 1, p. 175, (1921). https://dx.doi.org/10.1088/1478-7814/34/1/435

[38] R. L. Stenzel, J. Gruenwald, B. Fonda, C. Ionita, and R. Schrittwieser, " Transit time instabilities in an inverted fireball. I. Basic properties, " *Phys. Plasmas*, vol. 18, no. 1, p. 012104, (2011). https://doi.org/10.1063/1.3533437

[39] R. L. Stenzel, J. Gruenwald, B. Fonda, C. Ionita, and R. Schrittwieser, " Transit time instabilities in an inverted fireball. II. Mode jumping and nonlinearities, " *Phys. Plasmas*, vol. 18, no. 1, p. 012105, (2011). https://doi.org/10.1063/1.3533440

[40] R. L. Stenzel, and J. M. Urrutia , " Oscillating plasma bubbles. I. Basic properties and instabilities, " *Phys. Plasmas*, vol. 19, no. 8, p. 082105, (2012). https://doi.org/10.1063/1.4743019

[41] R. J. Taylor, K. R. MacKenzie, and H. Ikezi, "A Large Double Plasma Device for Plasma Beam and Wave Studies," *Rev. Sci. Instrum.* vol. 43, no. 11, p. 1675, 1972. https://dx.doi.org/10.1063/1.1685522

[42] D. Rafalskyi, and A. Aanesland, "Brief review on plasma propulsion with neutralizer-free systems," *Plasma Sources Sci. Technol.* vol. 25, no. 4, p. 043001, 2016. https://doi.org/10.1088/0963-0252/25/4/043001

[43] N. J. Mason, "The status of the database for plasma processing," *J. Phys. D: Appl. Phys.* vol. 42, no. 19, p. 083503, 2013. https://doi.org/10.1088/0022-3727/42/19/194003

[44] P. J. Kelly, and R. D. Arnell, "Magnetron sputtering: a review of recent developments and applications" *Vacuum*, vol. 56, no. 3, p. 159, 2000. https://dx.doi.org/10.1016/S0042-207X(99)00189-X

[45] P. Knoll, et al, "PECVD of carbon by inverted fireballs: From sputtering, bias enhanced nucleation to deposition," *Diam. Rel. Mater.*, vol. 65, p. 96, 2016. https://doi.org/10.1016/j.diamond.2016.02.021

[46] R. L. Stenzel, C. Ionita, and R. Schrittwieser, "Neutral gas dynamics in fireballs," *J. Appl. Phys.*, vol. 109, no. 11, p. 113305 , 2011. https://doi.org/10.1063/1.3594744

[47] J. Gilland, J. R. Breun, and N. Hershkowitz, "Neutral pumping in a helicon discharge," *Plasma Sources Sci. Technol.*, vol. 7, no. 3, p. 416, 1998. https://doi.org/10.1088/0963-0252/7/3/020

[48] A. Fruchtman, "Neutral gas depletion in low temperature plasma," *J. Phys. D: Applied Physics* vol. 50, no. 47, p. 473002, 2017. https://doi.org/10.1088/1361-6463/aa87a9

[49] R. L. Stenzel, W. Gekelman, N. Wild, J. M. Urrutia, and D. Whelan, "Directional velocity analyzer for measuring electron distribution functions in plasmas," *Rev. Sci. Instr* vol. 54, no. 10, p. 1302, 1983. https://dx.doi.org/10.1063/1.1137263

[50] R. L. Stenzel, "Ion Acceleration in Laboratory Plasmas," *Geophysical Monograph Series* vol. 38, p. 211, 1986. https://doi.org/10.1029/GM038p0211

[51] G. Fridman, et al, "Applied Plasma Medicine," *Plasma Process. Polym.*, vol. 5, no. 6, p. 503, 2008. https://doi.org/10.1088/1361-6595/aaa332

[52] R. L. Stenzel, "Method of and Apparatus for the electrostatic excitation of ions," *United States Patent* no. 4093856, 1978.

[53] J. Dawson, et al, "Isotope Separation in Plasmas by Use of Ion Cyclotron Resonance„" *Phys. Rev. Lett.* vol. 37, no. 23, p. 1547, 1976. https://doi.org/10.1103/PhysRevLett.37.1547

[54] R. L. Stenzel, "Whistler waves in space and laboratory plasmas," *J. Geophys. Res.*, vol. 104, no. 4, p. 14379, 1999. https://doi.org/10.1029/1998JA900120

[55] R. L. Stenzel, "Whistler waves with angular momentum in space and laboratory plasmas and their counterparts in free space," *Adv. Phys.-X* , vol. 1, no. 4, p. 687, 2016. https://doi.org/10.1080/23746149.2016.1240017

[56] J. M. Urrutia, R. L. Stenzel, and C. L. Rousculp, "Three-dimensional currents of

electrodynamic tethers obtained from laboratory models," *Geophys. Research Lett.* vol. 21, no. 6, p. 413, 1994. https://doi.org/10.1063/1.4795148

[57] R. L. Stenzel, and J. M. Urrutia, "A new method for removing the blackout problem on reentry vehicles," *J. Appl. Phys.* vol. 113, no. 10, p. 103303, 2013. https://doi.org/10.1063/1.4795148